AD-A064 095 AIR FORCE WEAPONS LAB KIRTLAND AFB N MEX F/G 18/8
THE EFFECTS OF WIND VARIABILITY OF NUCLEAR FALLOUT DOSES.(U)
AUG 78 L A WITTWER

UNCLASSIFIED AFWL-TR-78-64 SBIE-AD-E200 219 NL

1 OF 1
AD
A064095

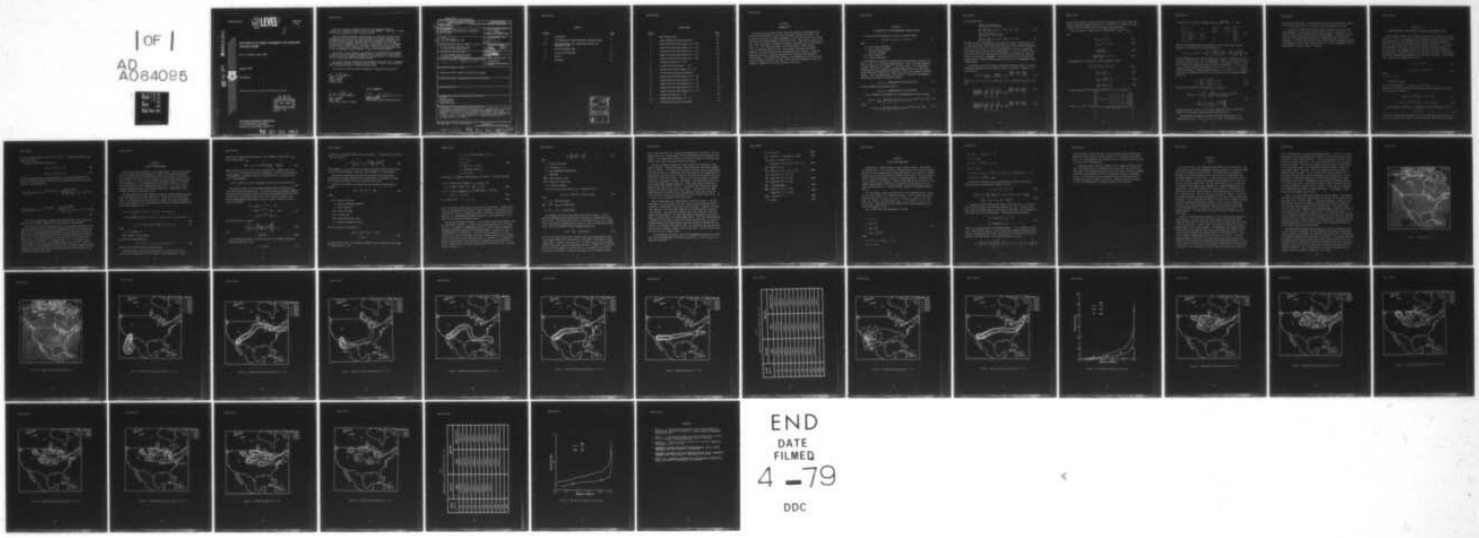

END
DATE
FILMED
4 -79
DDC

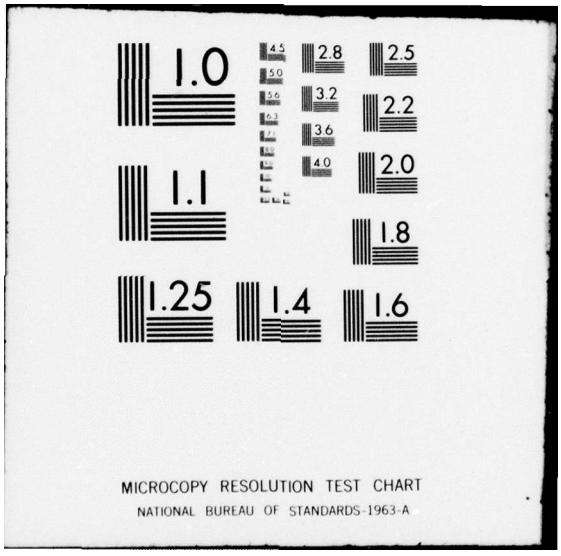
1.0
1.1
1.25
1.4
1.6
1.8
2.0
2.2
2.5
2.8
3.2
3.6
4.0
4.5
5.0
5.6
6.3
7.1
8.0
9.0
MICROCOPY RESOLUTION TEST CHART
NATIONAL BUREAU OF STANDARDS-1963-A

AFWL-TR-78-64

(2) LEVEL II

AFWL-TR-78-64

DDC ADE900217

AD A064095

DDC FILE COPY

THE EFFECTS OF WIND VARIABILITY ON NUCLEAR FALLOUT DOSES

Leon A. Wittwer, Capt, USAF

August 1978

Final Report

AIR FORCE WEAPONS LABORATORY
Air Force Systems Command
Kirtland Air Force Base, NM 87117

AFWL-TR-78-64

This final report was prepared by the Air Force Weapons Laboratory, Kirtland Air Force Base, New Mexico under Job Order 46950401. Capt Leon A. Wittwer (DYC) was the Laboratory Project Officer-in-Charge.

When US Government drawings, specifications, or other data are used for any purpose other than a definitely related Government procurement operation, the Government thereby incurs no responsibility nor any obligation whatsoever, and the fact that the Government may have formulated, furnished, or in any way supplied the said drawings, specifications, or other data is not to be regarded by implication or otherwise as in any manner licensing the holder or any other person or corporation or conveying any rights or permission to manufacture, use, or sell any patented invention that may in any way be related thereto.

This report has been reviewed by the Information Office (OI) and is releasable to the National Technical Information Service (NTIS). At NTIS, it will be available to the general public, including foreign nations.

This technical report has been reviewed and is approved for publication.

Leon A Wittwer

LEON A. WITTWER
Captain, USAF
Project Officer

FOR THE COMMANDER

John D Hawkins

JOHN D. HAWKINS
Major, USAF
Chief, Satellite and C^3 Branch

DERMOD KELLEHER
Deputy Chief, Applied Physics Division

UNCLASSIFIED

SECURITY CLASSIFICATION OF THIS PAGE (When Data Entered)

REPORT DOCUMENTATION PAGE

READ INSTRUCTIONS BEFORE COMPLETING FORM

1. REPORT NUMBER: AFWL-TR-78-64
2. GOVT ACCESSION NO.
3. RECIPIENT'S CATALOG NUMBER.

4. TITLE (and Subtitle): THE EFFECTS OF WIND VARIABILITY OF NUCLEAR FALLOUT DOSES
5. TYPE OF REPORT & PERIOD COVERED: Final Report
6. PERFORMING ORG. REPORT NUMBER

7. AUTHOR(s): Leon A. Wittwer, Capt, USAF
8. CONTRACT OR GRANT NUMBER(s): 47p.

9. PERFORMING ORGANIZATION NAME AND ADDRESS
Air Force Weapons Laboratory (DYC)
Kirtland Air Force Base, NM 87117

10. PROGRAM ELEMENT, PROJECT, TASK AREA & WORK UNIT NUMBERS
64711F
17 04
16 46950401

11. CONTROLLING OFFICE NAME AND ADDRESS
Air Force Weapons Laboratory (DYC)
Kirtland Air Force Base, NM 87117

12. REPORT DATE
11 August 1978
13. NUMBER OF PAGES
44

14. MONITORING AGENCY NAME & ADDRESS (if different from Controlling Office)
18 SBIE
19 AD-E200 219

15. SECURITY CLASS. (of this report)
UNCLASSIFIED

15a. DECLASSIFICATION/DOWNGRADING SCHEDULE

16. DISTRIBUTION STATEMENT (of this Report)

Approved for public release; distribution unlimited.

17. DISTRIBUTION STATEMENT (of the abstract entered in Block 20, if different from Report)

18. SUPPLEMENTARY NOTES

19. KEY WORDS (Continue on reverse side if necessary and identify by block number)
Fallout
Nuclear Effects
Wind Variability
Geostrophic Words

20. ABSTRACT (Continue on reverse side if necessary and identify by block number)
The effects of wind variability on nuclear fallout integrated doses is examined using recently developed Monte Carlo algorithms to generate sample three dimensional wind fields over the continental United States. Two scenarios are presented. The first is an intense attack on a proposed Advance Minuteman (MX) site near Yuma AZ. The second scenario is a lighter attack on the six Minuteman ICBM missile fields.

DD FORM 1 JAN 73 1473 EDITION OF 1 NOV 65 IS OBSOLETE

UNCLASSIFIED

SECURITY CLASSIFICATION OF THIS PAGE (When Data Entered)

CONTENTS

ILLUSTRATIONS

SECTION I

INTRODUCTION

The calculation of nuclear fallout doses and resulting casualties has been practiced by many people for many years using many different algorithms. One of the difficult areas in fallout assessments is the specification of wind fields required to calculate the paths of fallout particles. Many studies, particularly those with large numbers of weapons and targets, use mean winds or some "effective" wind. This is to allow calculation of fallout effects of large scenarios within a reasonable amount of time. Other studies, with much more modest scenarios, have used tabulated winds to determine fallout effects. Large data bases have been built containing measured wind fields over the Continental United States. The present effort presents a new methodology to arrive at wind fields for modest scenarios and takes a brief look at the adequacy of mean wind methods as compared to using more realistic wind fields.

SECTION II

THE GENERATION OF THREE-DIMENSIONAL CORRELATED WINDS

Let the wind be represented at a point by a complex number

$$w(x,y,z) = w_x(x,y,z) + i\, w_y(x,y,z) \tag{1}$$

where

x = west to east coordinate
y = south to north coordinate
z = vertical coordinate
w_x = west to east wind
w_y = south to north wind

It is assumed that the mean wind components are not contained in equation (1), hence, w_x and w_y are zero mean random variables. After w has been generated, the mean components can be added in to get total winds. It is furthermore assumed that w_x and w_y gaussian distributed random variables and the second order statistical processes with respect to w_x and w_y are stationary and homogeneous. With these assumptions, the statistics of the winds are completely described by the complex correlation function

$$G(\rho,\eta,\varepsilon) = \overline{w^*(x,y,z)\, w(x+\rho,\, y+\eta,\, z+\varepsilon)} \tag{2}$$

and the asymmetric correlation function

$$F(\rho,\eta,\varepsilon) = \overline{w(x,y,z)\, w(x+\rho,\, y+\eta,\, z+\varepsilon)} \tag{3}$$

Let us represent a wind pattern as a three-dimensional fourier integral.

$$w(x,y,z) = \frac{1}{(2\pi)^3} \int dk_x \int dk_y \int dk_z\; c(k_x,k_y,k_z)\, e^{\,i(k_x x + k_y y + k_z z)} \tag{4}$$

where

$$c(k_x,k_y,k_z) = \int dx \int dy \int dz\; w(x,y,z)\, e^{-i(k_x x + k_y y + k_z z)} \tag{5}$$

It can be shown that

$$\overline{c^*(k_x,k_y,k_z)\ c(k_x,k_y,k_z)} = \int d\rho \int d\eta \int d\varepsilon\ G(\rho,\eta,\varepsilon)\ e^{-i(k_x\rho + k_y\eta + k_z\varepsilon)} \tag{6}$$

$$\overline{c(k_x,k_y,k_z)\ c(-k_x,-k_y,-k_z)} = \int d\rho \int d\eta \int d\varepsilon\ F(\rho,\eta,\varepsilon)\ e^{-i(k_x\rho + k_y\eta + k_z\varepsilon)} \tag{7}$$

and that all other combinations of k_x,k_y, and k_z are zero. Equations (6) and (7) show that fourier coefficients correlate only in pairs mirrored through the origin of fourier space. It can also be shown that if w(x,y,z) is gaussian distributed, then so are the fourier coefficients. Finally, it follows that if two fourier coefficients are gaussian distributed and uncorrelated, then they are also statistically independent. By going to fourier space, the sampling problem has been reduced to sampling pairs of statistically independent complex random numbers.

In practice, the fourier integral expressions are approximated by discrete transforms evaluated using fast fourier transform algorithms. Equation (4) is now written as

$$w(x,y,z) = \frac{1}{8L_xL_yL_z} \sum_j \sum_k \sum_\ell c_{jk\ell}\ e^{i\left(\frac{j\pi x}{L_x} + \frac{k\pi y}{L_y} + \frac{\ell\pi z}{L_z}\right)} \tag{8}$$

where $-L_x \le x \le L_x$, $-L_y \le y \le L_y$, and $-L_z \le z \le L_z$. Equations (6) and (7) are now

$$\frac{\overline{C^*_{jk\ell}C_{jk\ell}}}{8L_xL_yL_z} \approx \int_{-L_x}^{L_x} d\rho \int_{-L_y}^{L_y} d\eta \int_{-L_z}^{L_z} d\varepsilon\ G(\rho,\eta,\varepsilon) e^{i\left(\frac{j\pi x}{L_x} + \frac{k\pi y}{L_y} + \frac{\ell\pi z}{L_z}\right)} \tag{9}$$

$$\frac{\overline{C_{jh\ell}C_{-j-k-\ell}}}{8L_xL_yL_z} \approx \int_{-L_x}^{L_x} d\rho \int_{-L_y}^{L_y} d\eta \int_{-L_z}^{L_z} d\varepsilon\ F(\rho,\eta,\varepsilon) e^{i\left(\frac{j\pi x}{L_x} + \frac{k\pi y}{L_y} + \frac{\ell\pi z}{L_z}\right)} \tag{10}$$

The only basic numerical restrictions on using equations (8)-(10) is that the spatial resolution adequately resolve $G(\rho,\eta,\varepsilon)$ and $F(\rho,\eta,\varepsilon)$ and that the aforementioned functions become small at the spatial mesh boundaries.

Let us now look at a specific pair of coefficients, $C_{jk\ell}$ and $C_{-j-k-\ell}$

Let

$$C_{jk\ell} = a_1 + i\, b_1 \tag{11}$$

$$C_{-j-h-\ell} = a_2 + i\, b_2 \tag{12}$$

$$\overline{C^*_{jk\ell}\, C_{jk\ell}} = K \tag{13}$$

$$\overline{C^*_{jh\ell}\, C_{-j-k-\ell}} = L + i\, M \tag{14}$$

From equations (11)-(14) with j, k and ℓ not equal to zero

$$\overline{a_1^2} = \overline{b_1^2} = \overline{a_2^2} = \overline{b_2^2} = K/2 \tag{15}$$

$$\overline{a_1 b_1} = \overline{a_2 b_2} = 0 \tag{16}$$

$$\overline{a_1 a_2} = \overline{-b_1 b_2} = L/2 \tag{17}$$

$$\overline{a_1 b_2} = \overline{a_2 b_1} = M/2 \tag{18}$$

The joint probability distribution function of a_1, a_2, b_1, and b_2 is

$$P(a_1, b_1, a_2, b_2) = C \exp\left\{ \frac{\left[\left| a_1\ b_1\ a_2\ b_2 \right| \begin{vmatrix} -K & 0 & -L & -M \\ 0 & K & -M & L \\ -L & -M & K & 0 \\ M & L & 0 & K \end{vmatrix} \begin{vmatrix} a_1 \\ b_1 \\ a_2 \\ b_2 \end{vmatrix} \right]}{(K^2 - L^2 - M^2)} \right\}$$

If a new set of variables is defined such that if $\sqrt{L^2 + M^2} = \sqrt{\quad}$ and

$$\begin{vmatrix} a_1 \\ b_1 \\ a_2 \\ b_2 \end{vmatrix} = \begin{vmatrix} 1 & 0 & -L/\sqrt{\quad} & -M/\sqrt{\quad} \\ 0 & 1 & -M/\sqrt{\quad} & L/\sqrt{\quad} \\ L/\sqrt{\quad} & M/\sqrt{\quad} & 1 & 0 \\ M/\sqrt{\quad} & -L/\sqrt{\quad} & 0 & 1 \end{vmatrix} \begin{vmatrix} a_1' \\ b_1' \\ b_2' \\ b_2' \end{vmatrix} \tag{20}$$

then after considerable matrix manipulation it can be shown that the joint probability distribution of the new variable set is

$$P'(a_1', b_1', a_2', b_2') = C' \exp\left\{ -\frac{1}{2}\left[\frac{2(a_1'^2 + b_1'^2)}{K + \sqrt{\quad}} + \frac{2(a_2'^2 + b_2'^2)}{K - \sqrt{\quad}}\right]\right\} \tag{21}$$

The new variable set can be easily sampled from a gaussian distribution because, as shown in equation (21), they are independent. After the new variable set has been sampled, the original set can be retrieved using equation (2) and $C_{jk\ell}$ and $C_{-j-k-\ell}$ can be calculated from equations (11) and (12). For $j = k = \ell = 0$, the sampling procedure is slightly different because $a_1 = a_2$ and $b_1 = b_2$. As before, a new set of independent coefficients can be found that can be sampled independently, Let

$$a_1 = \left[(K + L)/2\right]^{1/2}(a_1' + b_1') \tag{22}$$

$$b_1 \quad \left[(K - L)/2\right]^{1/2}(a_1' + b_1') \tag{23}$$

Then the joint probability distribution for a_1' and b_1' is

$$P(a_1', b_1') = C \exp\left\{ -\frac{1}{2}\left[\frac{2\left(K^2 - L^2 - M(K^2 - L^2)^{1/2}\right)}{K^2 - L^2 - M^2} a_1'^2 + \frac{2\left(K^2 - L^2 + M(K^2 - L^2)^{1/2}\right)}{K^2 - L^2 - M^2} b_1'^2\right]\right\} \tag{24}$$

Sample values for a_1 and b_1 can be found by sampling a_1' and b_1' according to equation (24) and then evaluating equations (22) and (23).

The procedure for generating a sample zero mean wind pattern can be summarized as follows. The $C_{jk\ell}$ for all j, k, and ℓ are sampled using the

procedures described above. The wind field is then found by evaluating equation (8). For the total wind field, the mean winds can be added to $w(x,y,z)$.

It was earlier assumed that the second order statistics of the wind field were homogeneous. This restriction can be easily relieved, particularly with respect to the standard deviation of the wind components. In practice the zero mean wind field is generated assuming unit standard deviation for both wind components. The final winds are calculated by multiplying the randomly generated wind components by their local standard deviations. Other inhomogeneties can be approximated in a similar manner if required.

SECTION III

THREE-DIMENSIONAL WIND CORRELATION FUNCTIONS FOR GEOSTROPHIC WINDS

The wind modeling used in this report requires the wind correlation functions. Buell (refs. 1 and 2) has developed several candidate horizontal wind correlation functions which do a very reasonable job in matching available measurements. There are two functions required to specify the wind correlations. The first is the longitudinal correlation function which describes the wind correlation at two points where the components sampled are parallel to the vector connecting the two points. The second function is the transverse correlation function where the sampled components are perpendicular to the connecting vector. The functions used, assuming unit standard deviation are

$$r_{\ell\ell'}(r) = e^{-\alpha^2 r^2/2} \tag{25}$$

$$r_{\ell\ell'}(r) = (1 - \alpha^2 r^2) e^{-\alpha^2 r^2/2} \tag{26}$$

where

$r = (\rho^2 + \eta^2)^{1/2}$

α = correlation length

The correlation length, α, is taken as 1.2×10^{-3} km^{-1}.
Equations (1) and (2) are easily converted to Cartesian coordinates and then to $F(\rho,\eta)$ and $G(\rho,\eta)$ functions

$$R(\rho,\eta) = e^{-\alpha^2 r^2/2} \left[2 - \alpha^2 (\rho^2 + \eta^2)\right] \tag{27}$$

$$S(\rho,\eta) = e^{-\alpha^2 r^2/2} \left[\alpha^2(\eta^2 - \rho^2) + 2i\, \alpha^2 \rho\eta\right] \tag{28}$$

For the vertical correlation, an exponential correlation function is used.

$$T(\varepsilon) = e^{-B\varepsilon} \tag{29}$$

This form is supported by Kochanski (ref. 3) who found that B varied from 0.08 to 0.14 km^{-1} during the Fall, Winter and Spring over the Continental United States.

During the summer B varied from 0.11 to 0.15 km^{-1}. For present purposes, B was taken to be 0.10 km^{-1}.

The total correlation functions are

$$G(\rho,\eta,\varepsilon) = R(\rho,\eta)\ T\ (\varepsilon) \tag{30}$$

$$F(\rho,\eta,\varepsilon) = S(\rho,\eta)\ T\ (\varepsilon) \tag{31}$$

The discussion on generating three-dimensional wind patterns showed that the fourier transforms of equations (30) and (31) are the quantities that are used directly. The transforms are

$$\int d\rho \int d\eta \int d\varepsilon\ G(\rho,\eta,\varepsilon) e^{-i(k_x\rho+k_y\eta+k_z\varepsilon)} = \frac{4\pi B e^{-\left(k_x^2+k_y^2\right)/2\alpha^2}}{\alpha^4\left(B^2+k_z^2\right)}\left(k_x^2+k_y^2\right) \tag{32}$$

$$\int d\rho \int d\eta \int d\varepsilon\ F(\rho,\eta,\varepsilon) e^{-i(k_x+k_y+k_z\varepsilon)} = \frac{4\pi B e^{-\left(k_x^2+k_y^2\right)/2\alpha^2}}{\alpha^4\left(B^2+k_z^2\right)}\left(k_y^2 - k_x^2 - 2i\,k_x\,k_y\right) \tag{33}$$

The first and second order statistics for the winds used in this study are from the Joint Strategic Target Planning Staff Climatic Wind Data Base.

This data base contains the mean west-east winds, the mean south-north winds, the major and minor axis of the elliptical standard deviation, and the rotation angle of the ellipse measured counterclockwise from the west-east direction for points on a latitude-longitude array and for altitudes ranging from sea level to about 20 km. The standard deviation ellipses over the U.S. are near circular with the major axis averaging 1.2 times the minor axis. The average of the rotation angle is near zero and the standard deviation is about 25°. Because of these properties of the standard deviation ellipses, the rotation angle is ignored except to calculate the west-east and south-north wind standard deviations used to normalize the random wind mesh.

SECTION IV

FALLOUT TRANSPORT MODEL

There are four basic elements to any transport model. They are the calculation of the amount and time dependence of the activity created, the particle size distribution, the activity per particle of a given size, and the fallout cloud dynamics. The first three are modeled with simple models that are physically reasonable but are not represented as particularly rigorous. The early time cloud dynamics is also modeled relatively simple. It is the late time transport where the natural wind field dominates that is emphasized. Each of the basic elements are discussed in turn.

The total amount of activity created is assumed to be 1500 roentgen per hour per kT per square mile at 1 hour after burst. If the burst is at the ground level, it is assumed that all the activity is lofted. For buried or elevated bursts, the lofted activity is decreased by the following fractions derived from dust lofting estimates (ref. 4).

$$F_\ell = 2.4 \times 10^{-6}\Big(112.5 + \Big((-9.11 \times 10^{-12} H^2 - 9.6 \times 10^{-6}) H^2 + 0.755\Big) H\Big)^2\Big(32.7 + \Big((1.78 \times 10^{-10} H^2 - 2.52 \times 10^{-5}) H^2 + 0.851\Big) H\Big) \quad H \leq 0 \tag{34}$$

$$F_\ell = 8.6 \times 10^{-8} (180-H)^2 (360 + H), \quad 0 < H \leq 180 \tag{35}$$

where

$$H = 3.28 \text{ (HOB) } W^{1/3}$$

HOB = height of burst (meters)

The activity time dependence is

$$f(t) = 2.76 \times 10\ \ t^{-1.23} - 2.39 \times 10^{4}\ t^{-1.45} \tag{36}$$

where f(t) is normalized to one at 3600 seconds.

The particle size distribution and the activity per particle of size r microns are assumed power law with indices n and m respectively. These

functions are combined and normalized to unity between a minimum scale, r_{min}, and a maximum scale, r_{max}.

$$M(r) = (m + n + 1)r^{m+n} / \left(r_{max}^{m+n+1} - r_{min}^{m+n+1}\right) \tag{37}$$

Nominal values for m and n are 2.7 and -4 respectively. Nominal values for r_{max} and r_{min} are 1000 and 0.5 microns respectively. The particle distribution is represented by a range of particles of decreasing size. The activity per micron is approximately

$$A(r,t) = 1500\ f(t)\ F_{\ell}\ M(r) \text{ (roentgens per hour per KT per square mile)} \tag{38}$$

The successive particle sizes representing the particle distribution are chosen starting at the largest size. The sizes are chosen to maintain adequate resolution over the particle size distribution and the downwind landing positions of particles of successively smaller size. Let us define a function, T(r), which is approximately proportioned to the fall time of a particle of size, r, from ten kilometers.

$$\begin{aligned} T(r) &= 6479.0\ r^{-1.9084}, \quad r < 105 \\ &= 383.1\ r^{-1.3008}, \quad 105 \leq r < 940 \\ &= 6.1527\ r^{-0.6973}, \quad 940 \leq r \end{aligned} \tag{39}$$

For particle indices, j, where

$$T^{-1}\left[T(r_j) + \left[\frac{\left(T(r_{NP}) - T(r_j)\right)}{NP - j}\right]\right] > B\ r_j \tag{40a}$$

and

$$T^{-1}\left[T(r)\right] = r \tag{40b}$$

r_{NP} represents the largest size group, and NP is the number of groups, r_j is chosen proportional to r_{j-1}.

$$r_j = r_{j-1}/B \tag{41}$$

Let the last index where equation (40) is true be m. All smaller particle group sizes are chosen by

$$r_j = T^{-1}\left[T(r_m) + (j-m)\,\frac{\left(T(r_{NP}) - T(r_m)\right)}{NP - m}\right] \tag{42}$$

The parameters, r_1, r_{NP}, NP, and B are chosen to maintain the specified resolution and include the range of particle sizes important in a given problem.

The particles representing the particle distribution are transported according to an assumed upward fallout cloud velocity, a calculated fall-rate, and a maximum achievable altitude in the random wind field.

Initially, each particle is assumed to rise according to the following equation.

$$H(t) = at^b,\ TST < t < TSR \tag{43}$$

where

H(t) = particle altitude

b = ALOG (H_i/RST)/ALOG (TSR/TST)

a = (RST + HOB)/TST^b

RST = initial altitude

TST = initial time

TSR = cloud stabilization time

H_i = maximum achievable altitude

The rise velocity of a particle is

$$V_r(t) = ab\,t^{b-1},\ TST < t \leq TSR$$
$$= 0,\ TSR < t \tag{44}$$

The particle fall rate is calculated as in DELFIC[5] with an extension of the model for large particles. Let

$$c_0 = r\,(\rho + 110.4)/(1.458 \times 10^{-6}\ \rho^{1.5})$$

$$c_1 = c_2\ r\ c_0$$

$$c_3 = c_0\ c_1\ \rho \qquad (45)$$

$$c_4 = \mathrm{LOG}_{10}\ (c_3) - 20.773$$

$$\rho = \text{air density } (kg/m^3)$$

$$c_2 = 3.4 \times 10^{-14}$$

The constant c_2 assumes a fallout density of 2.6 g/cm^3. The fall rates are

$$V_f = \left(1 + 0.233/(r\rho)\right)c_1 \left(41666.7 + c_3 \left(-2.3363 \times 10^2 + c_3\ (2.0154 - 6.9105 \times 10^{-3}\ c_3)\right)\right),\ c_3 < 140 \qquad (46a)$$

$$V_f = \left(1 + 0.233/(r\rho)\right)\left(50657.0\ c_1\right)\ c_3^{\left(0.0011235(c_4^2 - 443.98)\right)},$$

$$140 \leq c < 4.5 \times 10^7 \qquad (46b)$$

$$V_f = 0.294\ (r/\rho)^{1/2}, \qquad c_3 > 4.5 \times 10 \qquad (46c)$$

For V_f less than V_r, the particle rises with the rise velocity. As the particle rises, V_f increases and V_r decreases. After V_f exceeds V_r, the particle falls with velocity V_f until it reaches the ground. During the rise and fall of the particle, it is transported horizontally according to the random winds at the particles altitude and horizontal position.

The maximum achievable altitudes, H_i, are chosen to resolve the nuclear cloud at stabilization altitude. H_i varies from the cloud bottom, ACB, to the cloud top, ACT. The number of intermediate values of H_i, NLVL, chosen to guarantee reasonable downwind resolution of the fallout pattern. A particle of size r is transported for each value of H_i. To account for the activity for a given particle size, A(r,t) of equation 38 must be divided according to H_i to reflect the division of the fallout cloud into layers. In addition, it is necessary to account for the radius of the cloud which is needed to calculate the activity due to a given particle size from a given layer of the fallout cloud. The cloud radius at time t_ℓ, is

$$R_\ell = \left[\left(c\ t_s^d\right)^2 = Dt_\ell\right]^{1/2} \tag{47}$$

where

t_ℓ = particle land time

t_s = time when $V_f = V_r$

d = ALOG (RMAX/RMIN)/ALOG(TSR/TST)

$c = RMAX/TSR^d$

RMAX = stabilization radius

RMIN = radius at initial time

D = diffusion constant

The activity per micron given H_i for t greater than t_ℓ is

$$A(r,t,H_i) = 1500\ f(t)\ F_\ell\ M(r)\ G_i/(\pi R_\ell^2) \tag{48}$$

where

$G_1 = (H_2 - ACB)/\left(2(ACT-ACB)\right)$

$G_{NLVL} = (ACT - H_{NLVL-1})/\left(2(ACT-ACB)\right)$

$G_i = (H_{i+1} - H_{i-1})/\left(2(ACT-ACB)\right)$

The transport now can be summarized by the following steps. A set of particles representing the particle size distribution is transported with H_i equal to ACB. The landing points define a line called a trace. Next, another set of particles are transported with H_i equal to ACB + DLVL defining a second trace. DLVL is the nominal distance between successive H_i.

$$DLVL = (ACT - ACB)/(NLVL-1) \tag{49}$$

Next for each landing point of the second trace, the minimum distance to the first trace divided by the cloud radius is calculated. The maximum of these values, DMAX, is stored in an array, FLVL, if larger than one, and the landing points of the second trace are permanently retained. If DMAX is less than one the last trace is ignored. In either case, H_i is increased by DLVL and the next trace is calculated. Traces are calculated for the selected H_i with H_i

equal to ACT being the last. By picking reasonable NLVL, hence DLVL, this procedure results in a minimum number of traces representing the downwind fallout pattern. The landing points defining the traces are stored in a transport data base for each burst to be assessed later for analysis.

The above transport procedure can become expensive if there are a large number of bursts. There are two model simplications that can greatly expedite the calculations. If the scenario has groups of similar bursts at approximately the same time within a limited area, then these groups can be represented by a single group cloud whose radius is equal to the radius of the area of the burst group plus a single burst radius. The activity of the new cloud is increased according to the number of bursts in the group. The second simplication is to use an abbreviated transport algorithm. Three traces are calculated with H_i equal to ACB, (ACB + ACT)/2, and ACT. The middle traces defines the landing positions and times for the final single trace. The cloud radius for each landing point on the middle trace is the average of the distances from the first and third trace to the landing point plus the original cloud radius. All of the activity is assigned to the single trace.

Both of these models cost some accuracy in the final results. The group cloud smears out the fallout in the local area of the bursts and the loss of resolution is determined by the original burst locations. Downwind, the group cloud smearing is not significant compared to the uncertainties in multiple cloud dynamics. The simplified transport model loses resolution within the downwind fallout pattern. This model does deposit approximately the correct amount of fallout within the correct downwind area. Thus, the simplified model is adequate for statistical studies and limited transport times. It must be abandoned when the increased internal resolution of specific patterns are required or the transport times get too long. The resolution available with the multiple level transport is about a local cloud radius. This is the best available with any disk transport model.

In the preceding discussion, values of the parameters dealing with the fallout cloud were enumerated but not numerically defined. The fits used in this model are as follows:

$$TST = 0.15\ W^{0.333} \tag{50a}$$

$$RST = 150.0\ W^{0.333} + \text{Maximum}\ (0.0,\ HOB) \tag{50b}$$

$$TSR = 418.0 - 120.0\ W^{0.5},\ W < 1$$

$$= 20.0(16.0 + 6.0\ \log_{10}(W) - W^{0.27}),\ W \geq 1 \tag{50c}$$

$$ACB = 1800.0,\ W < 1.5$$

$$ACB = 1447.0\ W^{0.5385},\ 1.5 \leq W < 10.0 \tag{50d}$$

$$ACB = 3263.0\ W^{0.1854},\ 10.0 \leq W$$

$$ACT = 4674.0\ W^{0.3080},\ W < 10.0 \tag{50e}$$

$$ACT = 6210.0\ W^{0.1846},\ W \geq 10.0$$

$$NLVL = (ACT-ACB)/1000.0 \tag{50f}$$

$$RMAX = 2553.0\ W^{0.2310},\ W < 30.0$$

$$= 1884.0\ W^{0.3203}\ \ W \geq 30.0 \tag{50g}$$

$$RMIN = 150.0\ W^{0.333} \tag{50h}$$

$$D = 100.0 \tag{50i}$$

SECTION V

FALLOUT DATA PROCESSING

Fallout data is usually desired in one of several formats. Three formats are available here. The first format involves contours of the mean and standard deviation of the integrated dose at specified times for the scenario of interest. Contours are also available for each different wind pattern. The second format supplies the man and standard deviation of integrated dose for selected times for an inputted list of targets. The last format supplies the statistics of the number and percentage of United States population of integrated dose at geographic points supplied by a population model supplied by the RAND Corporation (ref. 6).

All three formats require the calculation of the integrated dose at a point from which trace data in the transport data base. Let us consider the landing points of particles of sizes, r_{i+1} and r_i, at times, t_{i+1} and t_i, with cloud radii, R_{i+1} and R_i, with activities, $A(r_{i+1}, t_{i+1}, H)$ and $A(r_i, t_i, H)$, on a single trace. These quantities are assumed to vary linearly between the end points with respect to time.

Let us define the linear dependence as follows:

$$\begin{aligned} x &= a_x t + b_x \\ y &= a_y t + b_y \\ R &= a_R t + b_R \\ A &= (a_A t + b_A)\, f(t) \end{aligned} \tag{51}$$

where

$$a_x = (x_{i+1} - x_i)/(t_{i+1} - t_i)$$

$$b_x = x_i - a_x t_i$$

$$a_y = (y_{i+1} - y_i)/(t_{i+1} - t_i)$$

$$b_y = y_i - a_y t_i$$

$$a_R = (R_{i+1} - R_i)/(t_{i+1} - t_i)$$

$$b_R = R_i - a_R t_i$$

$$a_A = A(r_{i+1}, t_{i+1}, H)/f(t_{i+1}) - A(r_i, t_i, H)/f(t_i)/(t_{i+1} - t_i)$$

$$b_A = A(r_i, t_i, H)/f(t_i) - a_A t_i$$

In order for a point (x_o, y_o) to be affected by fallout, the following condition must be true for some t between t_i and t_{i+1}.

$$(x - x_o)^2 + (y - y_o)^2 \leq R^2 \tag{52a}$$

$$t^2\left[a_x^2 + a_y^2 - a_R^2\right] + t\left[2a_x(B_x - x_o) + 2a_y(b_y - y_o) - 2a_R b_A\right] + \left[(b_x - x_o)^2 + (b_y - y_o)^2 - b_R^2\right] = 0 \tag{52b}$$

In general, equation (52b) has zero, one, or two roots for t. If there is one or less roots, then no fallout has landed at (x_o, y_o). If there are two roots, then the fallout depends on the values of the roots. Let the large and small roots be t_ℓ and t_s respectively. Then redefine these quantities.

$$t_\ell = \text{minimum } (t_\ell, t_{i+1}, T)$$
$$t_s = \text{maximum } (t_s, t_i) \tag{53}$$

where T is the sample time for the integrated dose. If t_s is greater or equal to t_ℓ, then no fallout occurs. If not, then there is some contribution to the fallout. Assuming that the fallout is uniformly distributed in the horizontal direction, the contribution to the integrated dose at x_o, y_o is

$$D_s = \left(\frac{r_{i+1} - r_i}{t_{i+1} - t_i}\right) \int_{t_s}^{t_\ell} dt \left(A \int_t^T du\, u\, f(u) + b_A \int_t^T du\, f(u)\right) \tag{54}$$

The first factor on the right side is used to maintain proper normalization because the outer integral is better thought of as an integral over particle size. D_s is calculated for each successive pair of locations along each trace to get the total integrated dose.

To maintain proper resolution transverse to the general direction of the trace, the traces must not be separated by more than the local cloud radius. The traces in the transport data base are not that close. To maintain adequate resolution, pseudo traces are linearly interpolated between the calculated traces. This procedure maintains reasonable resolution without having to transport an excessive number of particles. Where the simplified transport is used, no interpolation is required as there is only one trace.

SECTION VI

RESULTS

Two scenarios were run to demonstrate the effects of wind variability. The first scenario involved 7000 one-megaton warheads targeted on a proposed advanced missile (MX) complex near Yuma, Arizona. The second scenario targeted the Minuteman Missile (MM) complexes on the great plains with approximately two one-megaton weapons per missile silo. In both cases group clouds were used for each local complex. Thus one cloud modeled the MX problem and six clouds, one for each wing, were used for MM. The cloud radii were all set at sixty miles. The remaining cloud dynamics were identical to a single one-megaton burst at ground level. The fission fraction of all bursts was 0.5. The particle size distribution and other necessary details were discussed earlier in the transport or wind sections. The wind statistics used were for January. The correlation lengths and other statistical properties of the wind field were previously discussed. Figure 1 shows the mean winds for January at two kilometers altitude. The winds trend toward the east as expected. Figure 2 shows a sample wind pattern at the same altitude where the variability effects have been added. This pattern shows typical circulatory wind patterns characteristic of real weather patterns. It is the effects of these circulatory features that are under study.

Figures 3-7 show sample dose patterns for five different wind patterns for the MX scenario. Figure 8 shows the fallout pattern using the mean winds. Comparison shows that real winds can carry fallout to regions that would not be covered by mean winds. Figure 9 shows the average dose contours for the two hundred cases run for the MX scenario. The roughness of the contours indicate that even the large number of cases used give only moderate averages at the low dose levels indicating the residual effects of high variability. A more useful comparison between mean and variable winds is in table 1. The table shows the number and percent of the United States population exposed to the listed dose for the mean and variable winds with the standard deviation for the variable winds. The most obvious significantly underestimated by the mean wind calculation. This is caused by the winds taking the patterns occasionally over

heavily populated areas raising the mean expected doses. This effect is clearly accentuated by the high strength fallout source in a localized area which leads to very long intense fallout patterns. Figure 10 demonstrates the most extreme case out of the two hundred runs. This case exposed over fifty million people to more than 1300 R. This very high casualty count was caused by three factors. First, the fallout cloud did not appreciably disperse laterally. Second, the cloud rapidly moved to the east. Lastly, the pattern went over the heavily populated eastern corridor. This is a very extreme case as shown by fig. 11 which shows the cumulative casualty distribution for the MX scenario. There is only about a three percent chance that the population exposed to over 1300 R would exceed ten million. The skewness of the cumulative distribution results in the mean casualties at a given level as shown in table 1 differing from the 50 percent probability casualty count in figure 11. Also shown is a comparison with a RAND calculation (ref. 6) at the 1300 R level. The agreement is good considering the modeling uncertainties.

Figures 12-16 shows sample dose patterns for the MM scenario. The patterns from each field are now much shorter because the sources are now spread out with less total yield. Figure 17 shows the mean wind calculation. Again the variability causes regions to be exposed that otherwise would not be. Figure 18 shows the mean dose averaged over fifty different winds. The smooth contours with less cases clearly demonstrates the decreased impact of the wind variability with dispersed sources. Table 2 repeats table 1 for the MM calculations. In this case comparison between the mean wind dose and the mean dose over winds show little difference. Figure 19 shows the cumulative casualty distribution for MM. The curves are nearly linear over most of the range which is consistent with the expected casualties at a given level on table 2, being approximately equal to the 50 percent probability casualty count.

The two scenarios indicate that the impact of variability decreases as the fallout sources are dispersed. For the MX scenario, the intense concentrated source resulted in long patterns which lead to high variability in the casualties as the patterns wandered over large areas of the country. For the more dispersed MM scenario, the individual patterns were smaller, decreasing the variability. The implication is clear that for many widely dispersed sources such as massive laydowns, the wind variability effects can be ignored and mean winds used for casualty assessments. Only in localized or very intense scenarios with long patterns does wind variability appear to be significant.

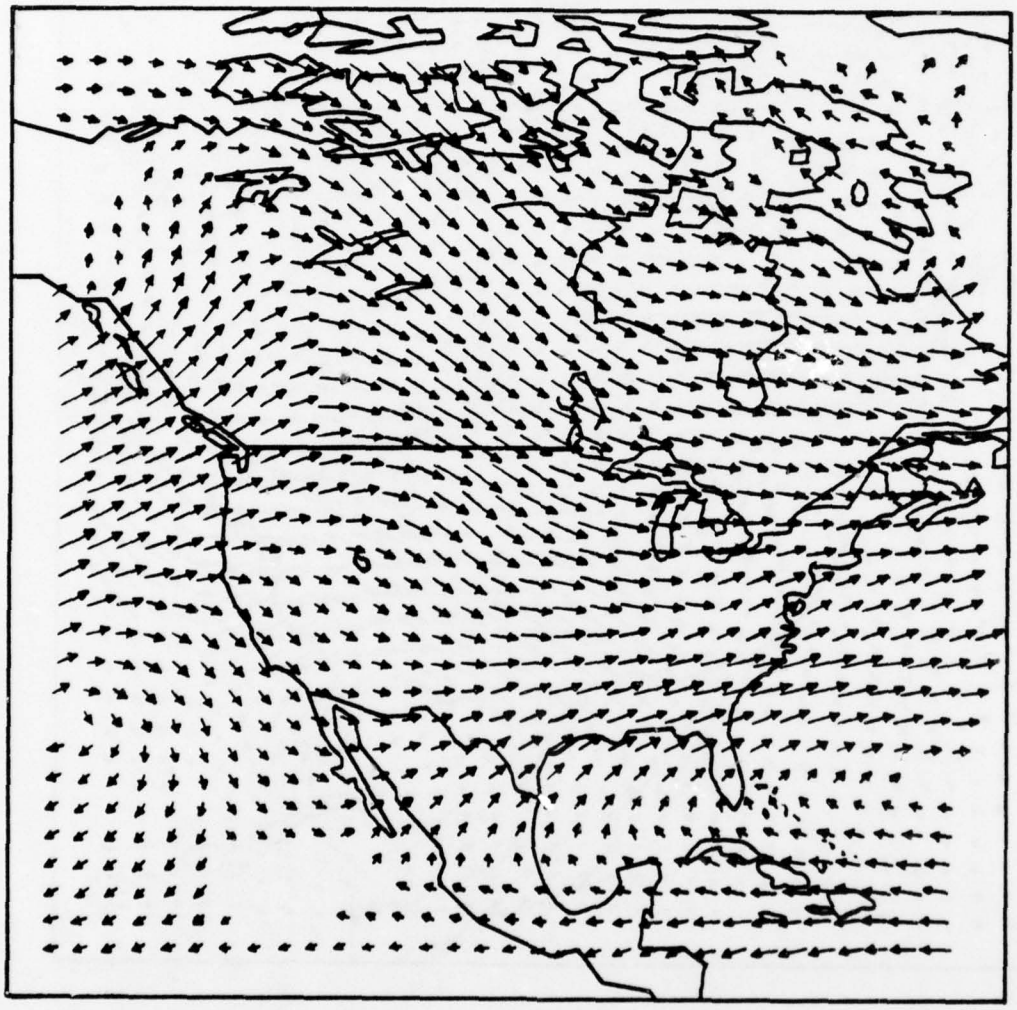

Figure 1. Mean January Winds

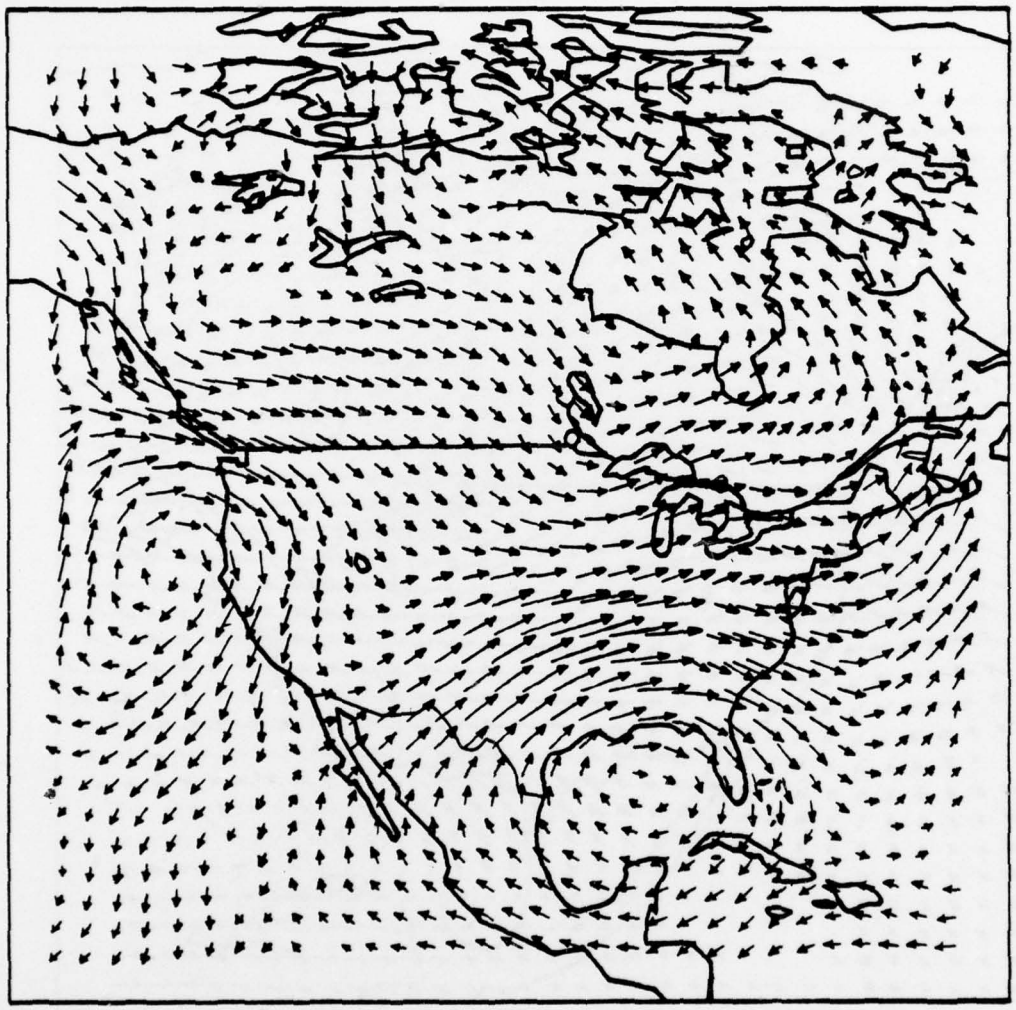

Figure 2. Sample January Wind With Variability

Figure 3. Sample MX Fallout Dose Contours at T = 10^8

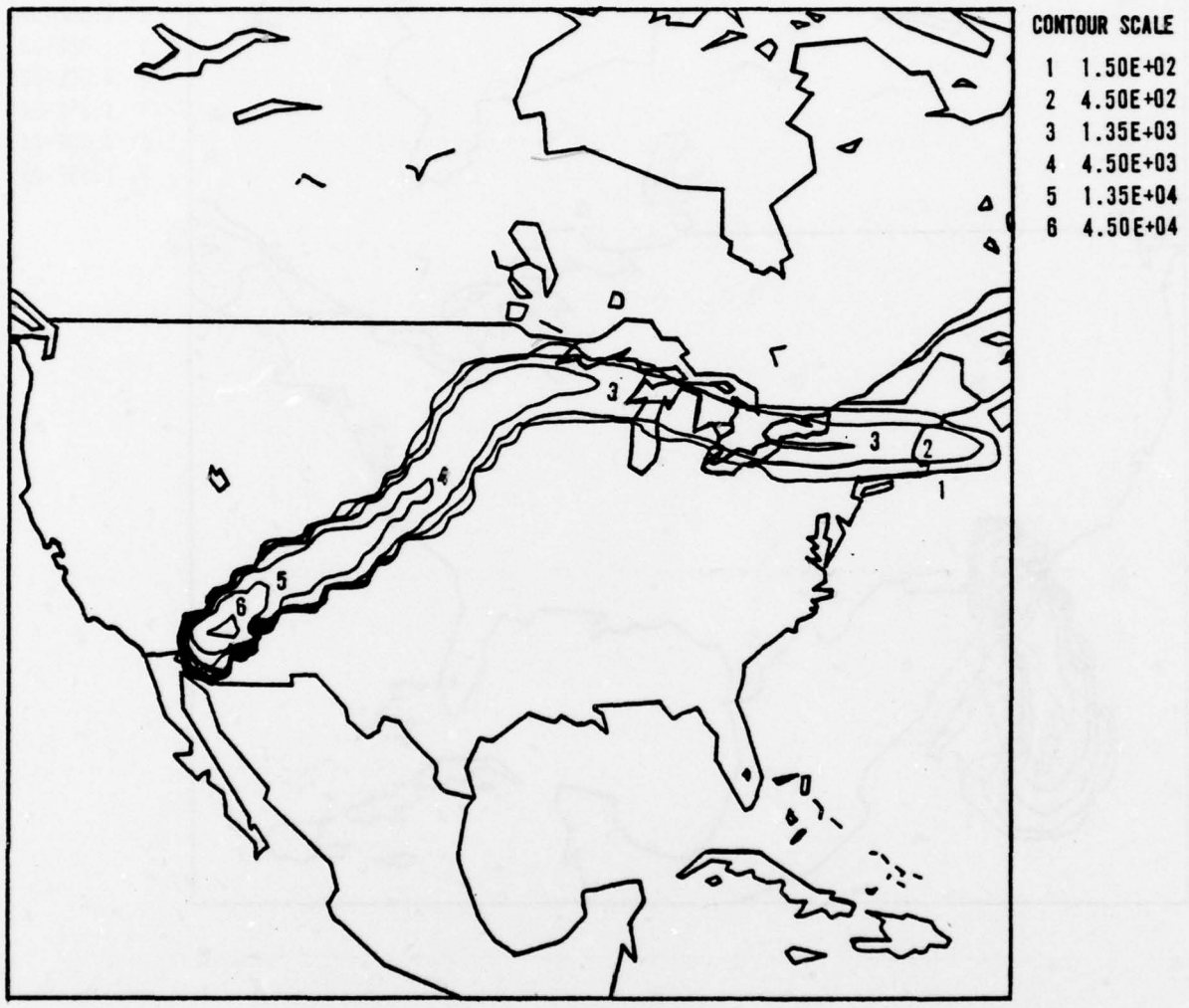

Figure 4. Sample MX Fallout Dose Contours at T = 10^8

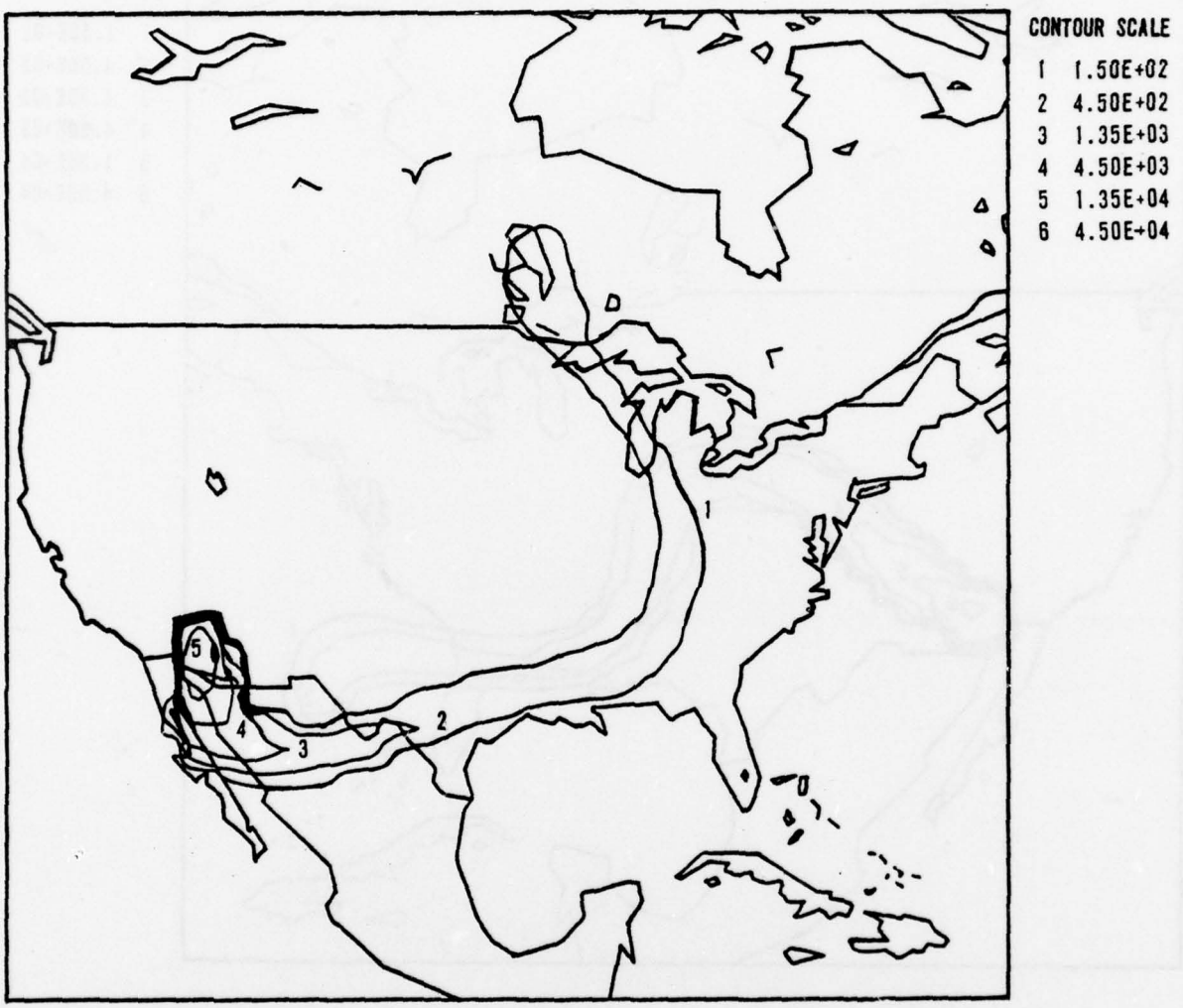

Figure 5. Sample MX Fallout Dose Contours at T = 10^8

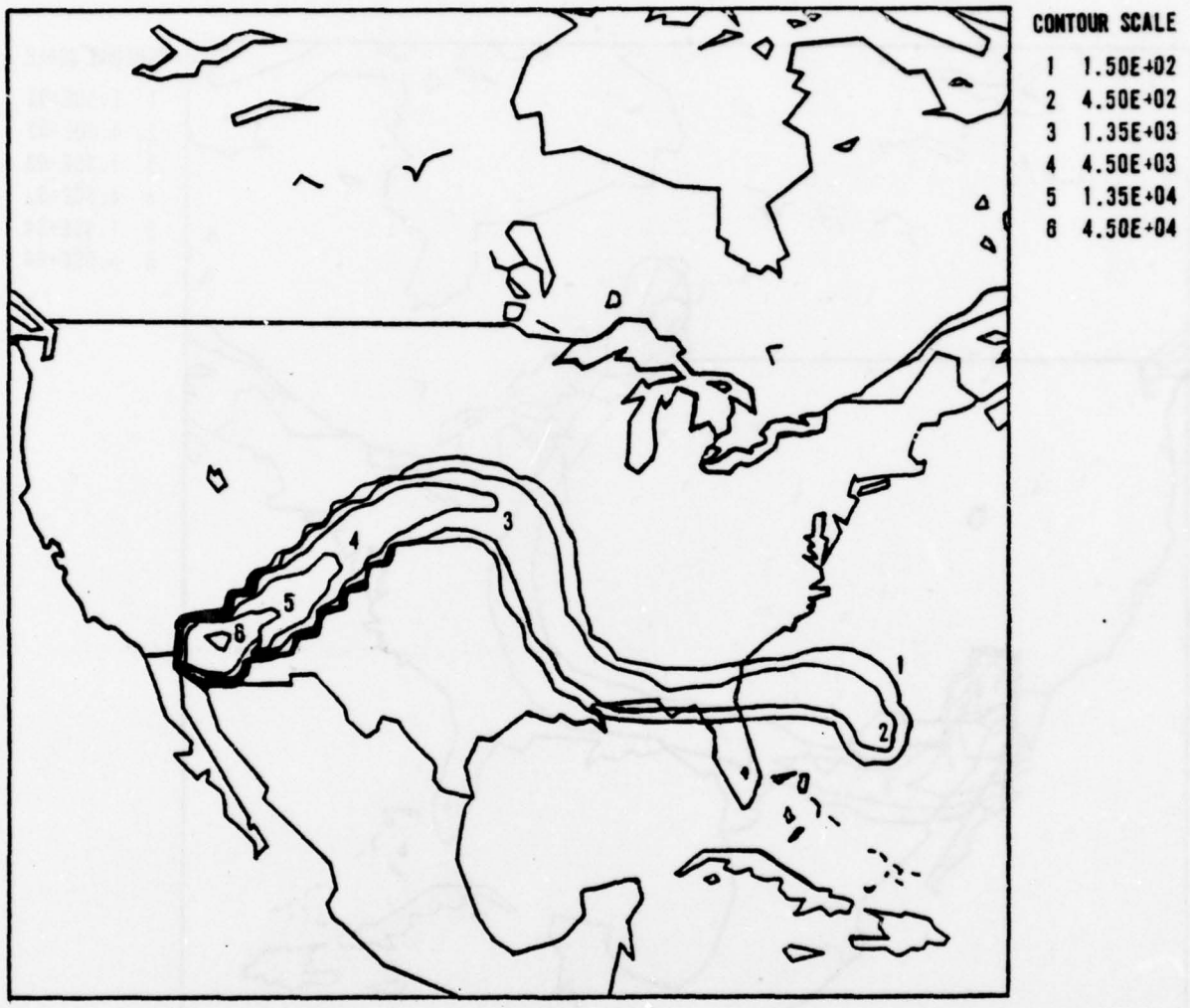

Figure 6. Sample MX Fallout Dose Contours at T = 10^8

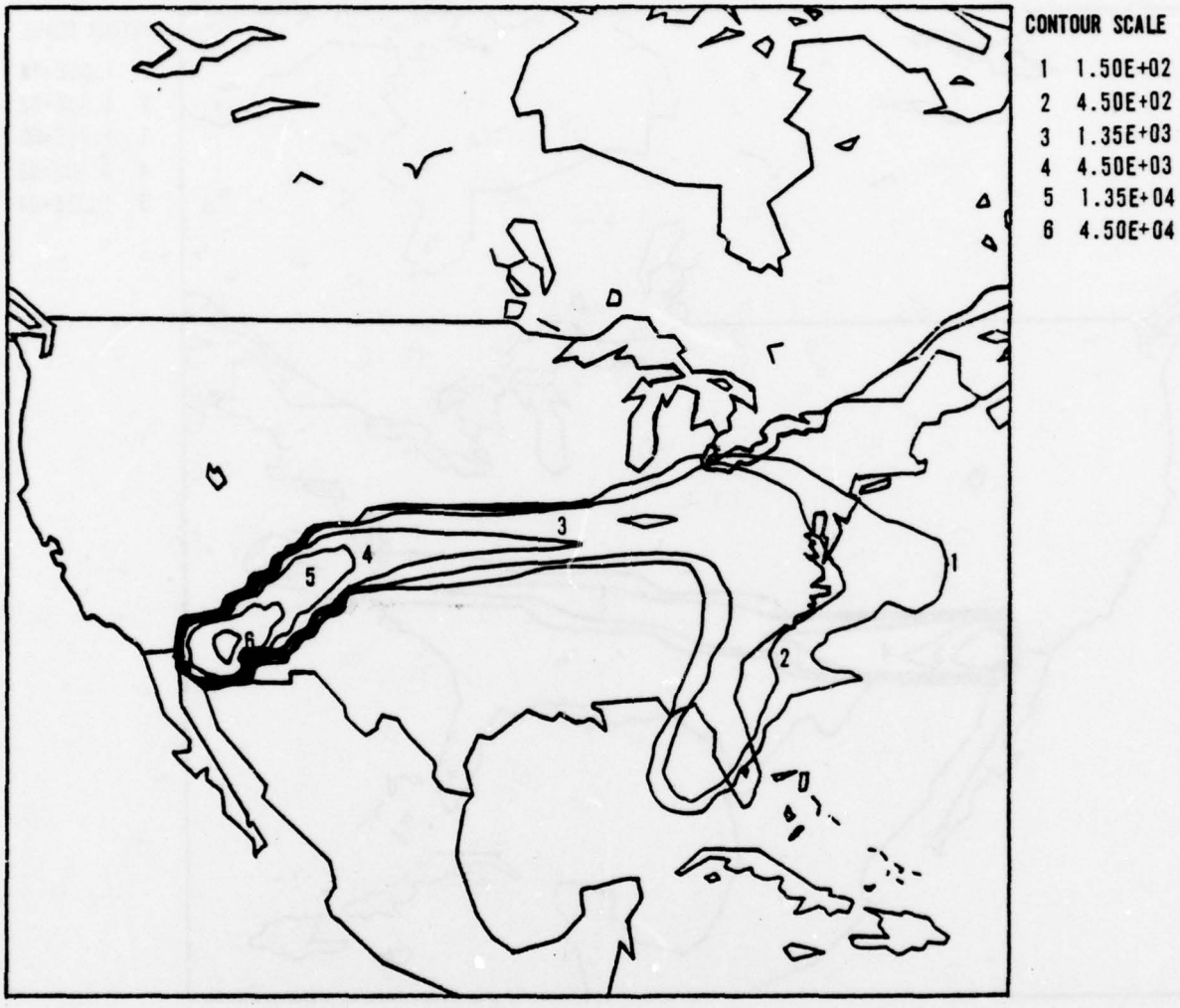

Figure 7. Sample MX Fallout Dose Contours at $T = 10^8$

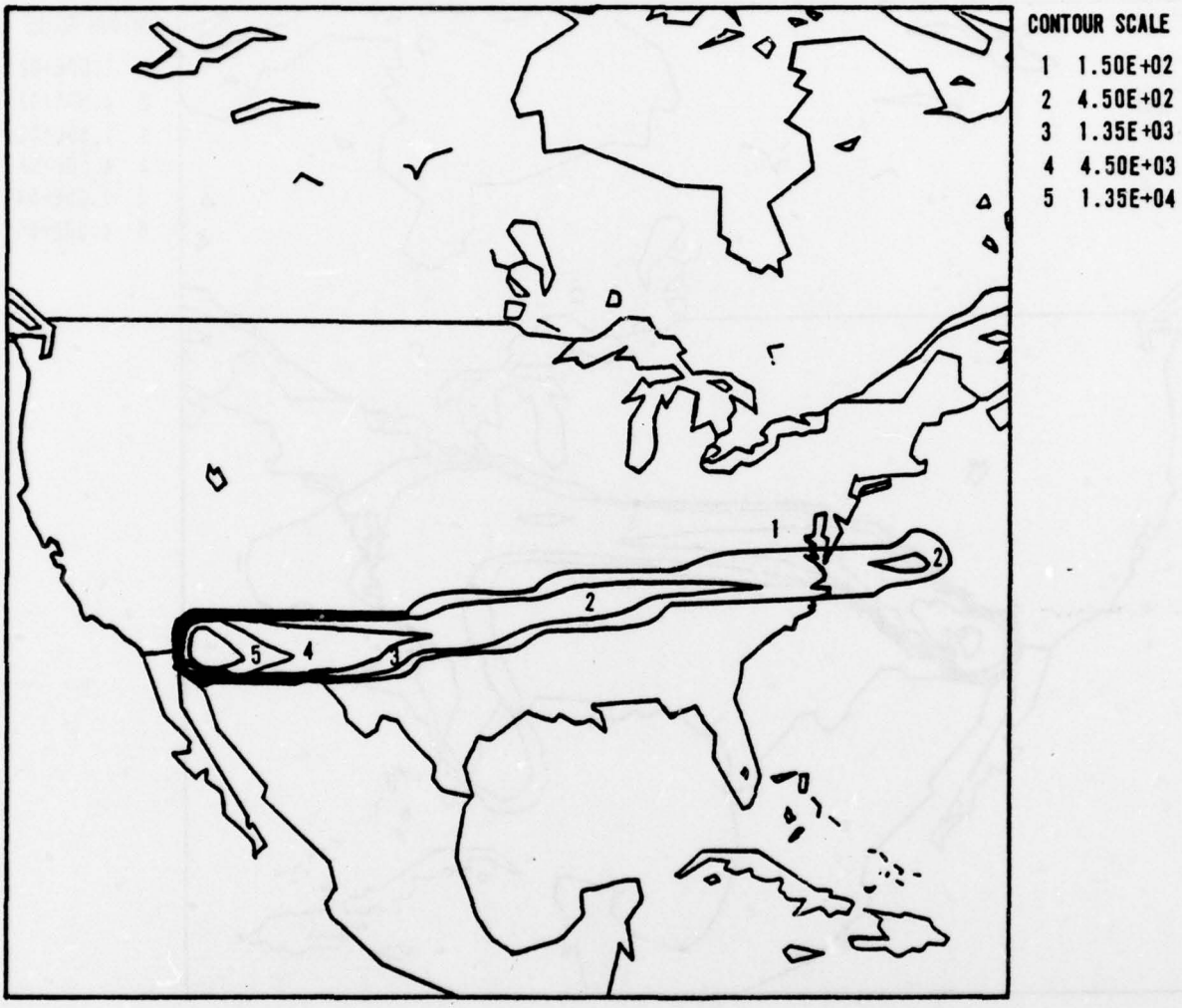

Figure 8. MX Mean Wind Dose at T = 10^8

Table 1

NUMBER/PERCENT OF POPULATION EXPOSED AT TIME = 10^8

MINIMUM DOSE (R)	MEAN WINDS	RANDOM WINDS	
	AVERAGE	AVERAGE	STANDARD DEVIATION
100	$1.5X10^7/7.3$	$3.1X10^7/15.3$	$2.2X10^7/10.8$
170	$1.4X10^7/6.8$	$2.2X10^7/10.8$	$1.7X10^7/8.4$
280	$1.3X10^7/6.4$	$1.7X10^7/8.1$	$1.4X10^7/6.7$
460	$8.1X10^6/4.0$	$1.1X10^7/5.3$	$1.0X10^7/5.0$
770	$3.3X10^6/1.6$	$6.4X10^6/3.2$	$7.2X10^6/3.5$
1300	$1.5X10^6/0.7$	$3.2X10^6/1.6$	$4.5X10^6/2.2$
2200	$1.1X10^6/0.5$	$1.5X10^6/0.7$	$2.0X10^6/1.0$
3600	$9.0X10^5/0.5$	$8.3X10^5/0.4$	$7.5X10^5/0.4$
6000	$9.0X10^5/0.5$	$6.3X10^5/0.3$	$4.9X10^5/0.2$
10000	$8.0X10^5/0.4$	$5.2X10^5/0.3$	$4.0X10^5/0.2$
130000		$6.7X10^3/\sim 0$	$5.3X10^4/\sim 0$
1000000			

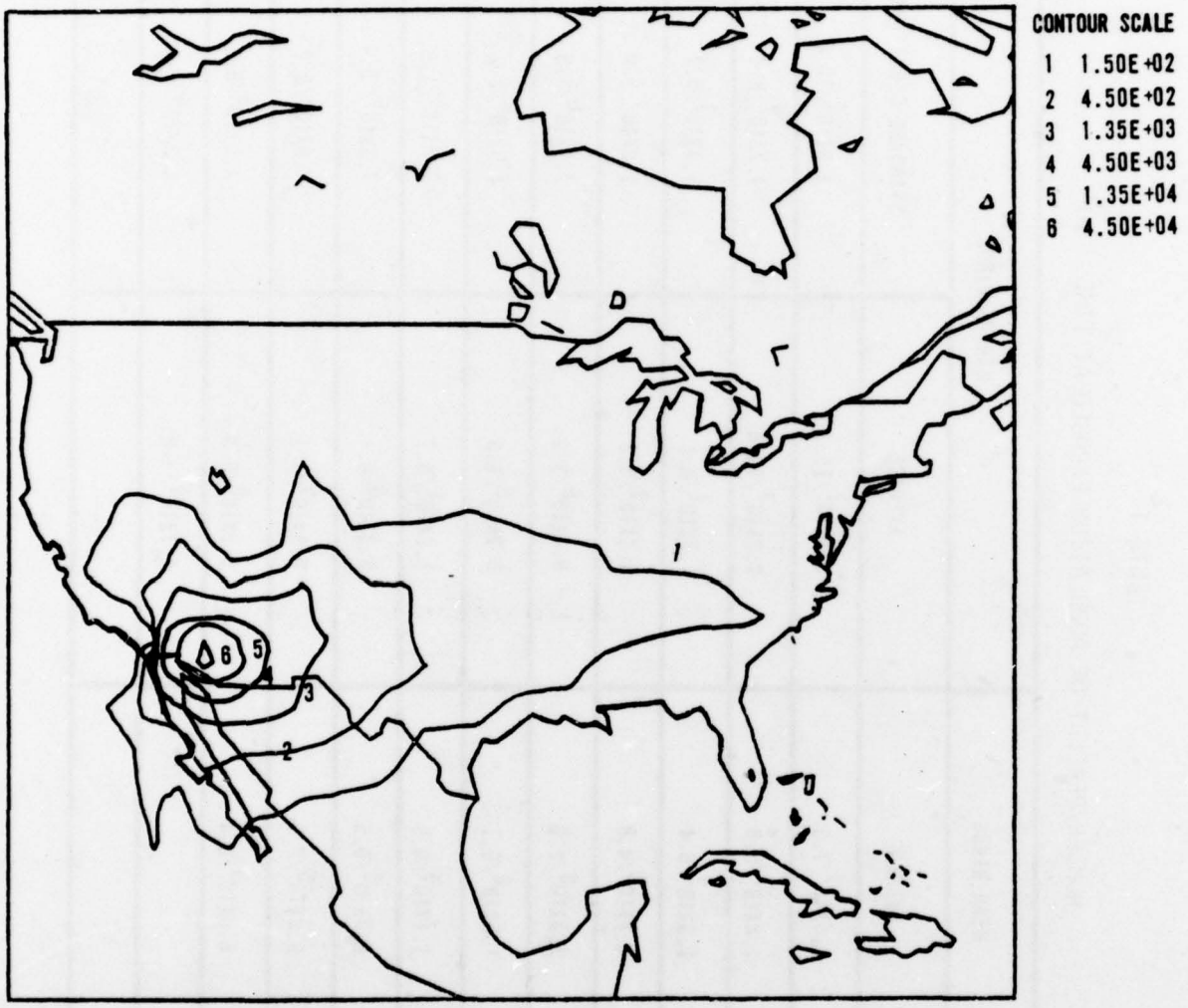

Figure 9. MX Mean Over Winds Dose at T = 10^8

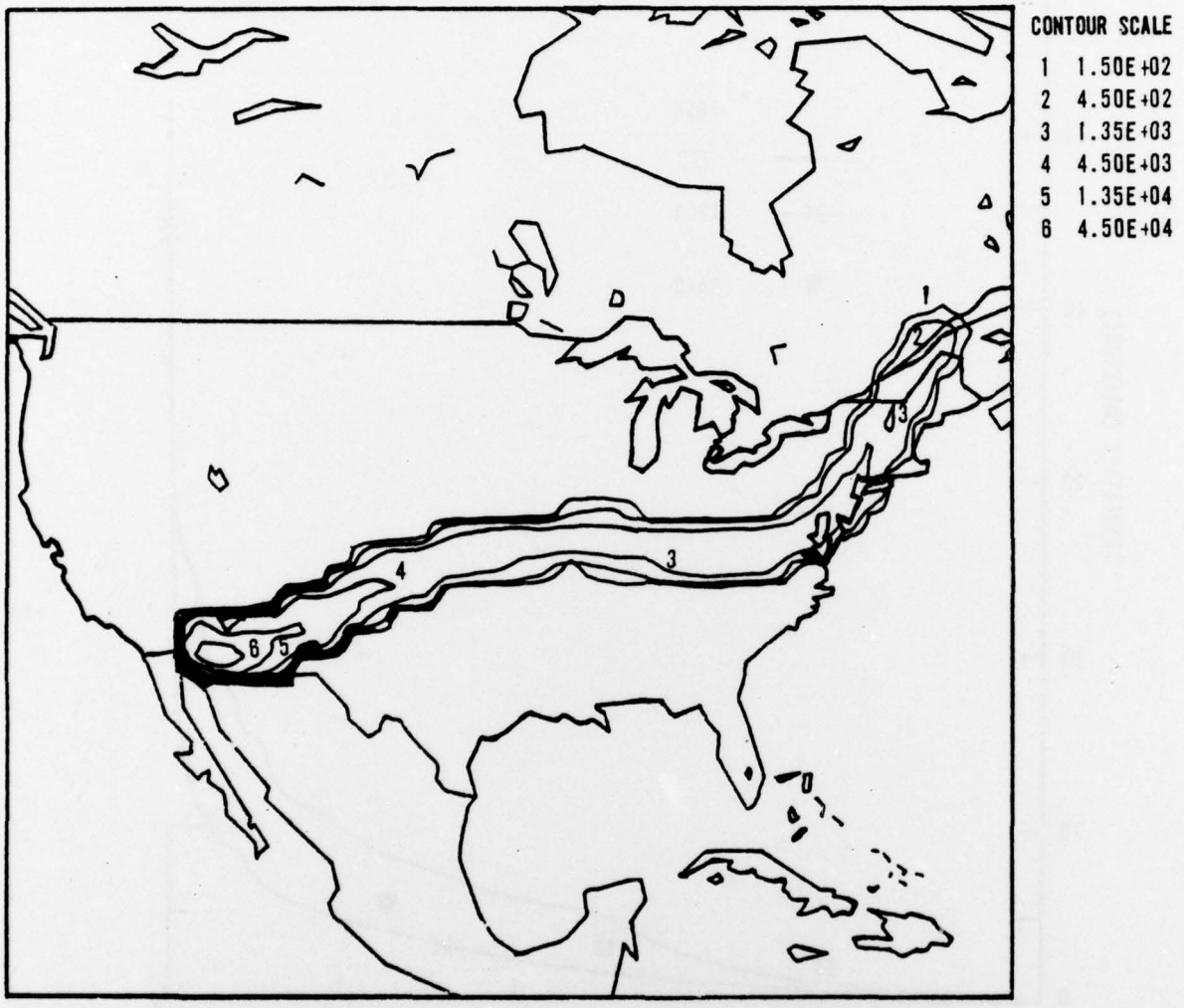

Figure 10. 60th MX Fallout Dose Contour at T = 10^8

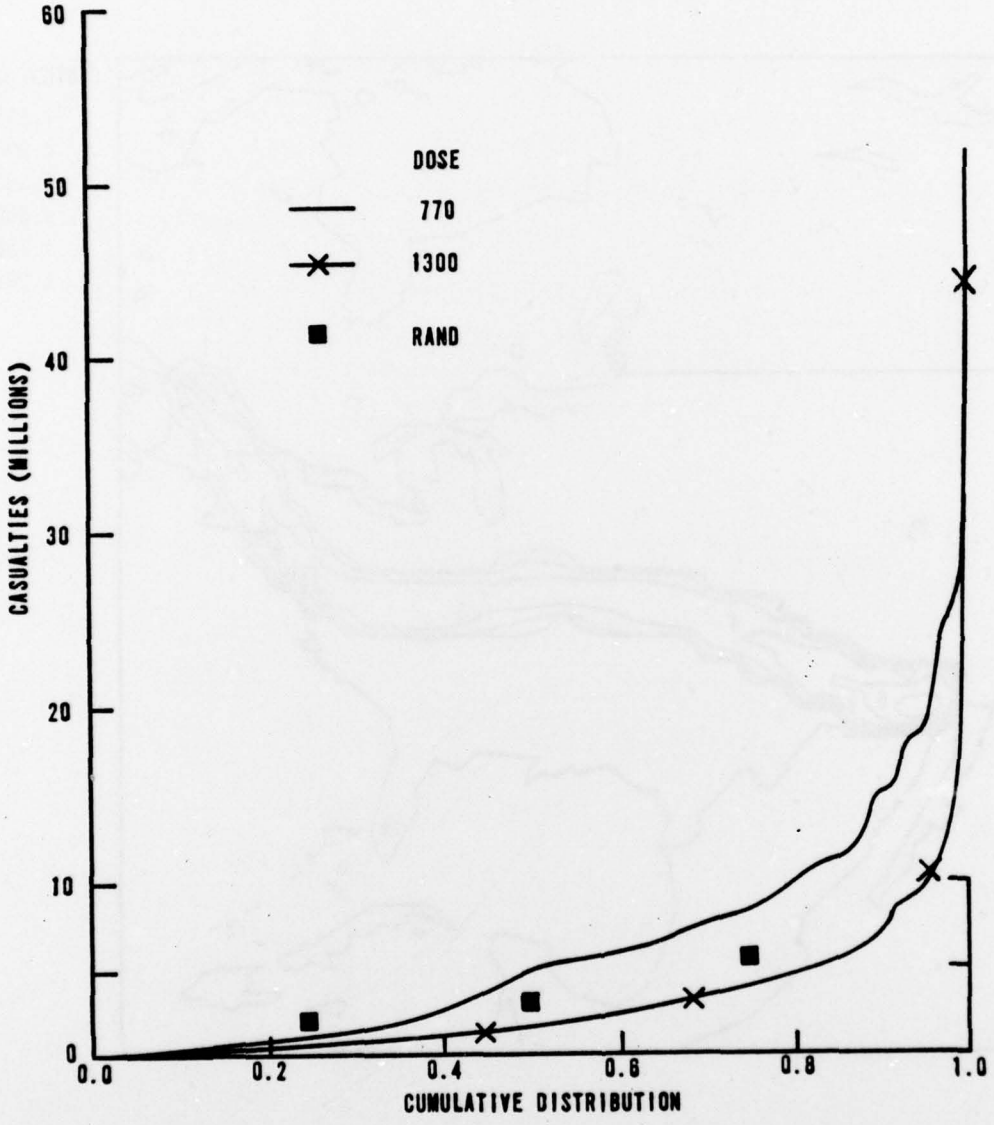

Figure 11. MX Cumulative Casualty Distribution

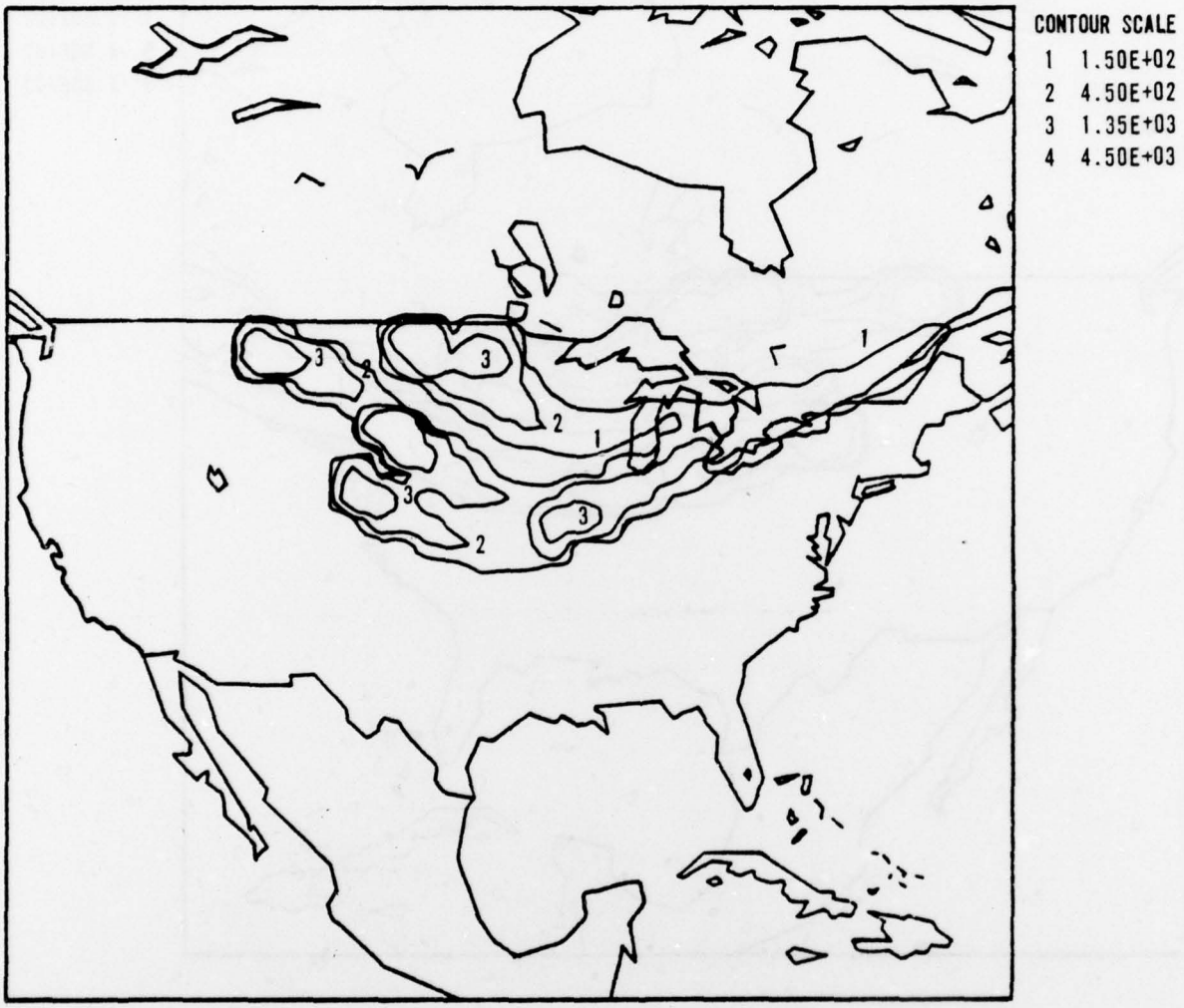

Figure 12. Sample MM Fallout Dose Contours at T = 10^8

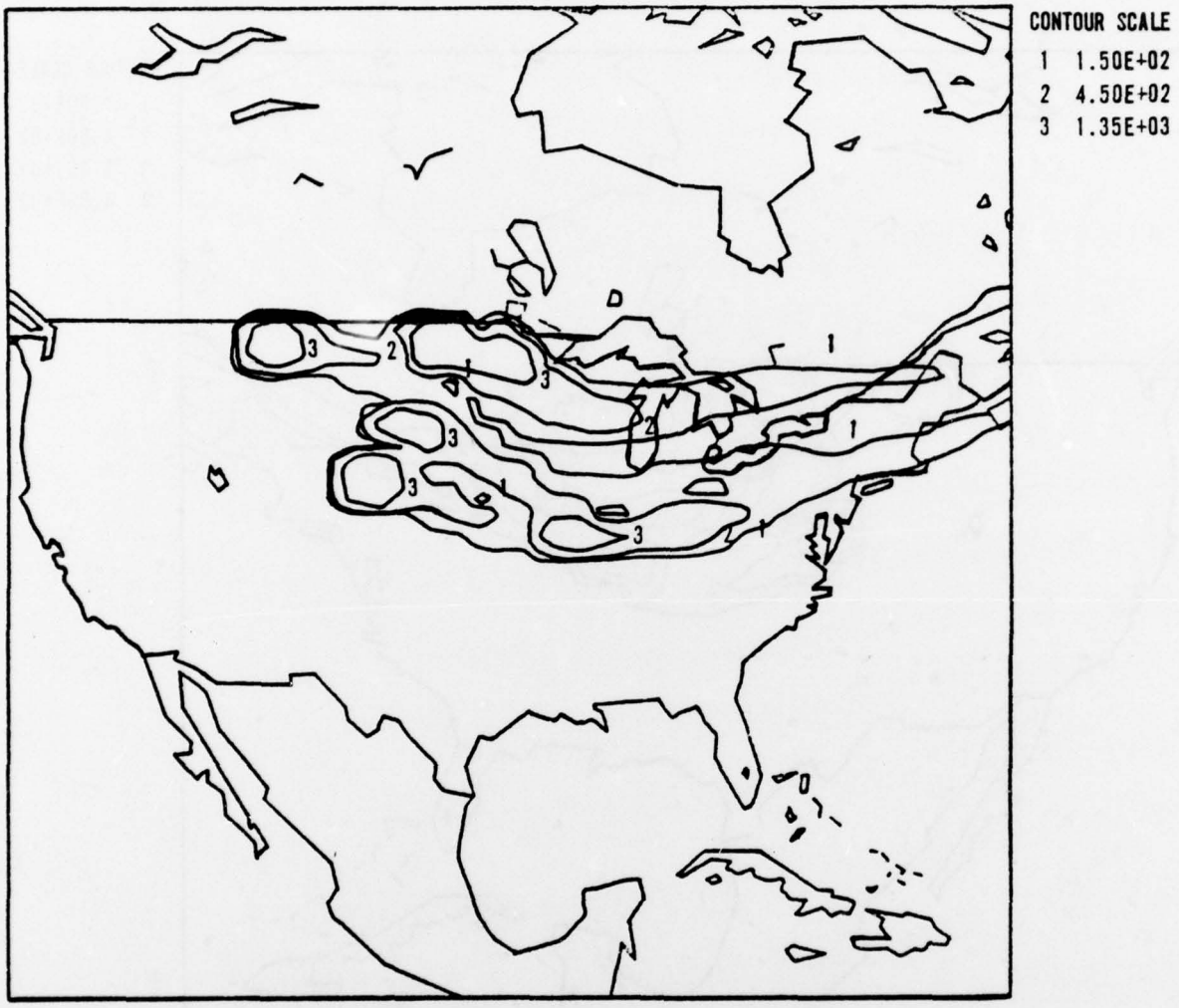

Figure 13. Sample MM Fallout Dose Contours at T = 10^8

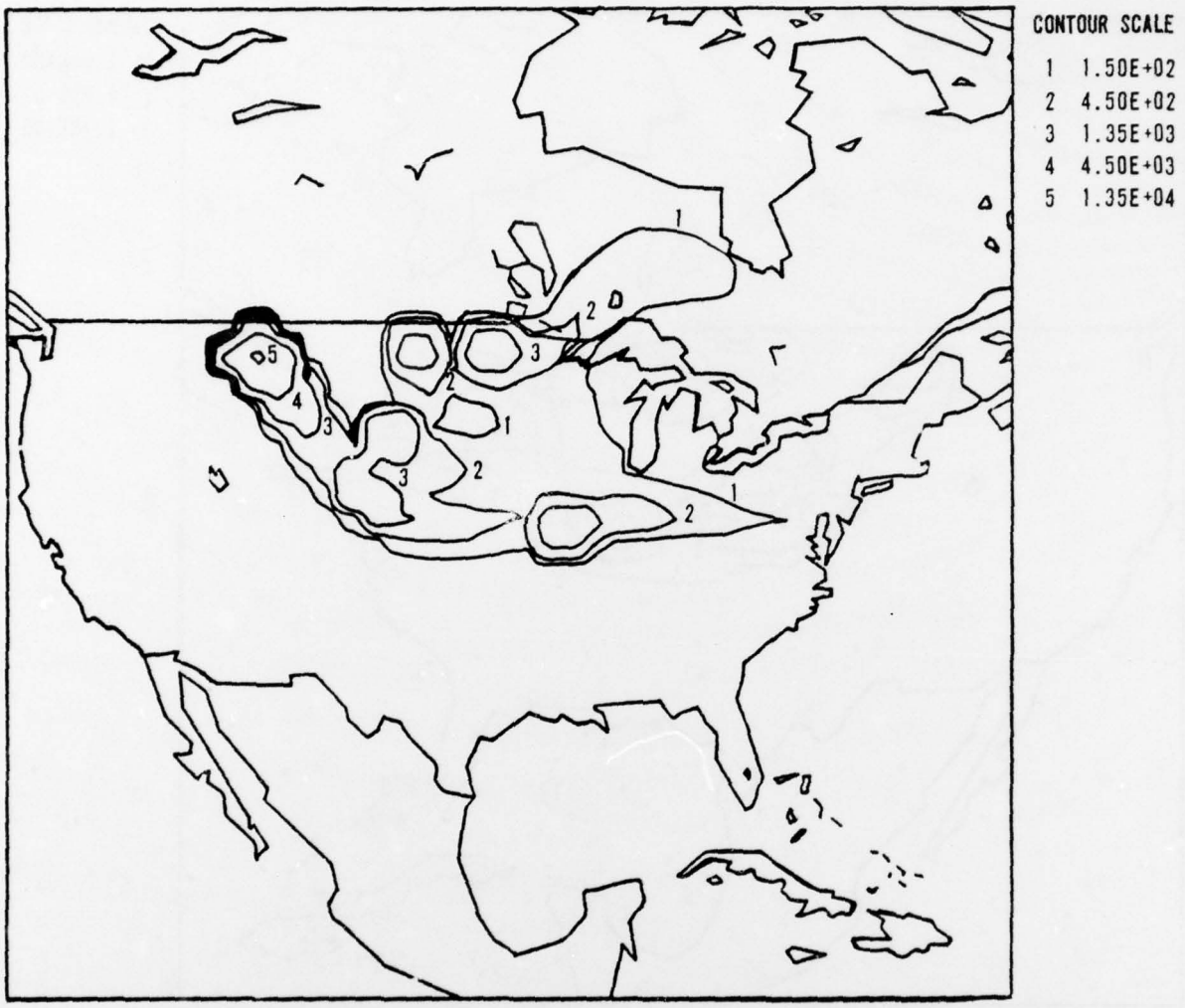

Figure 14. Sample MM Fallout Dose Contours at T = 10^8

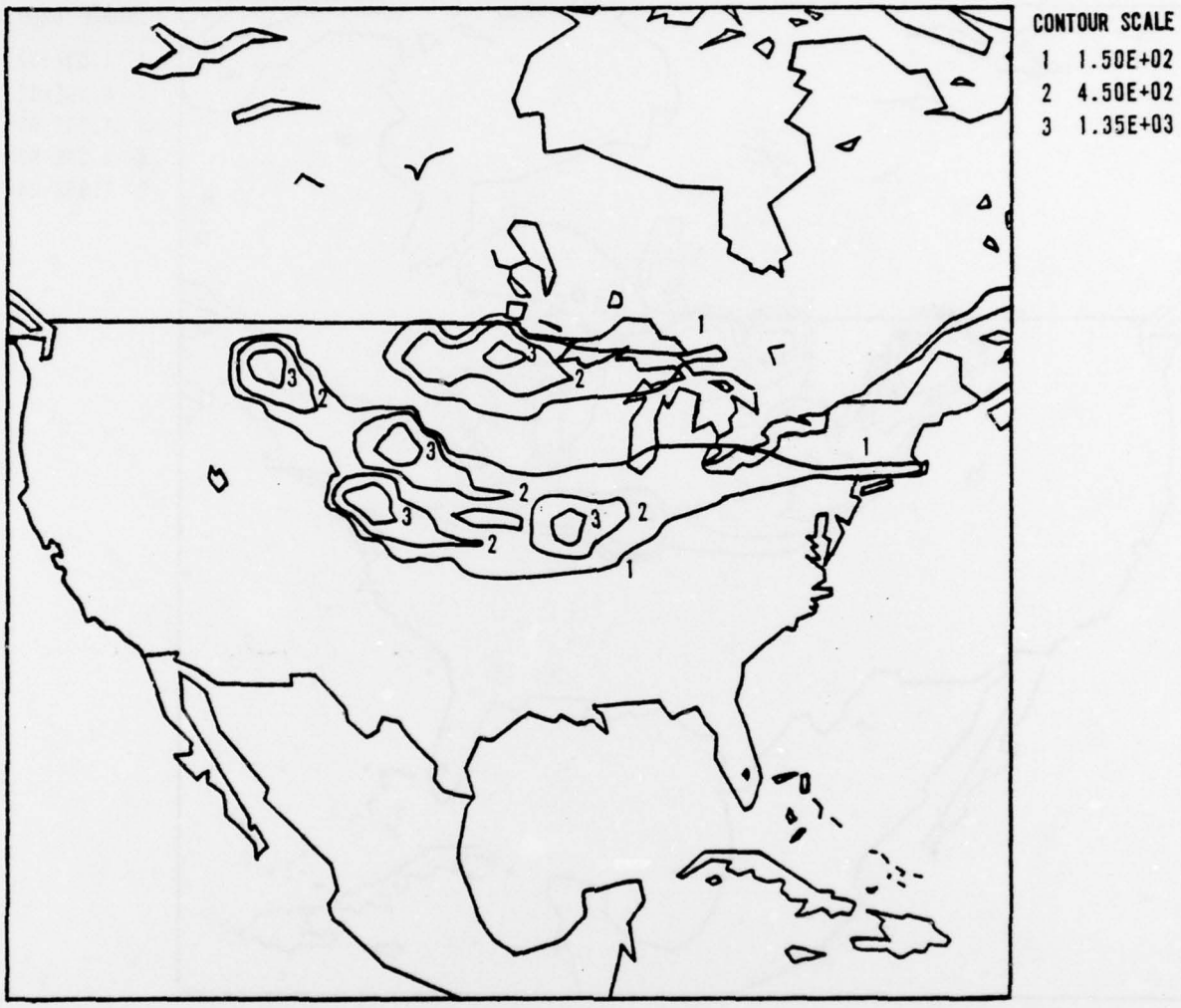

Figure 15. Sample MM Fallout Dose Contours at T = 10^8

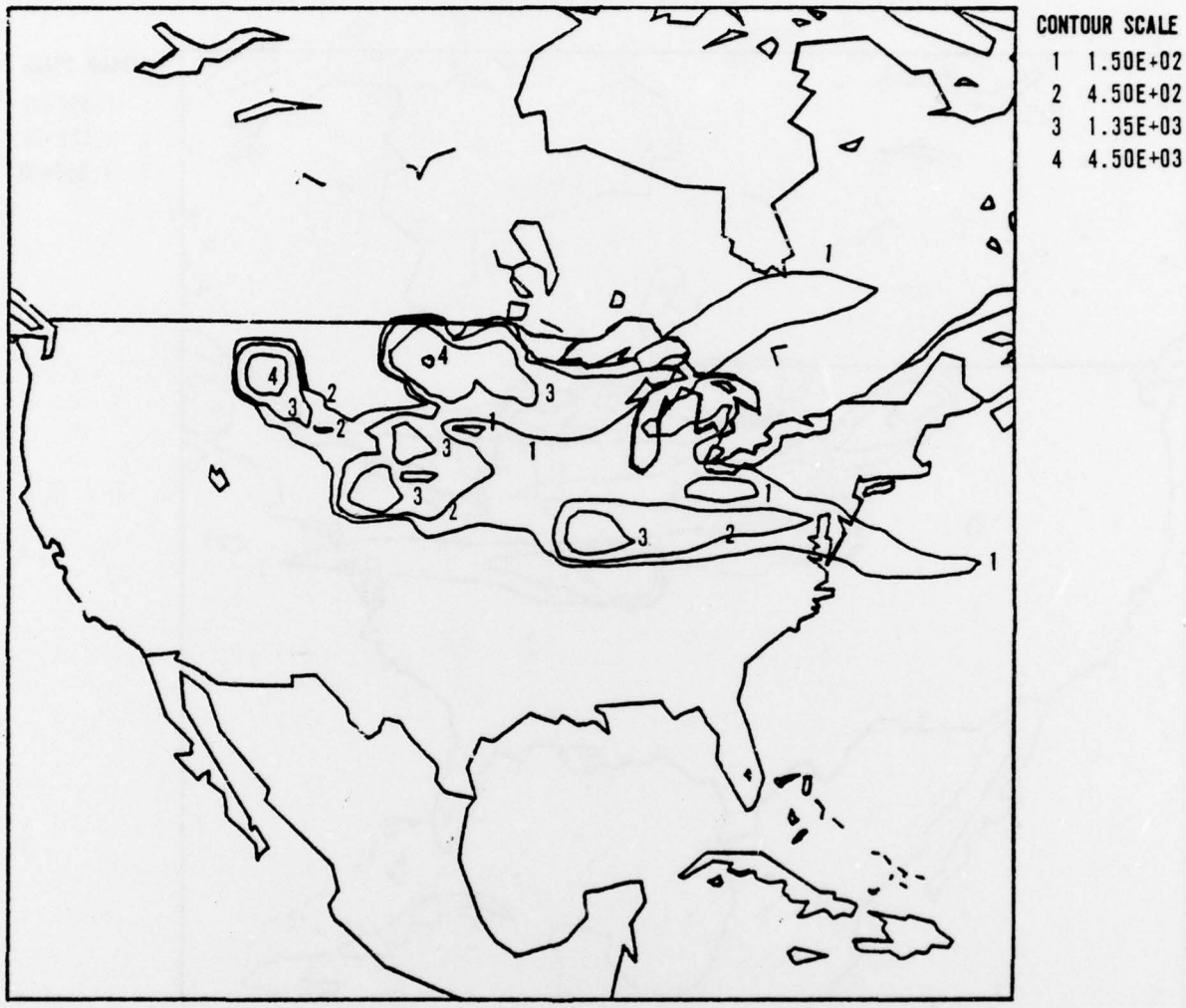

Figure 16. Sample MM Fallout Dose Contours at T = 10^8

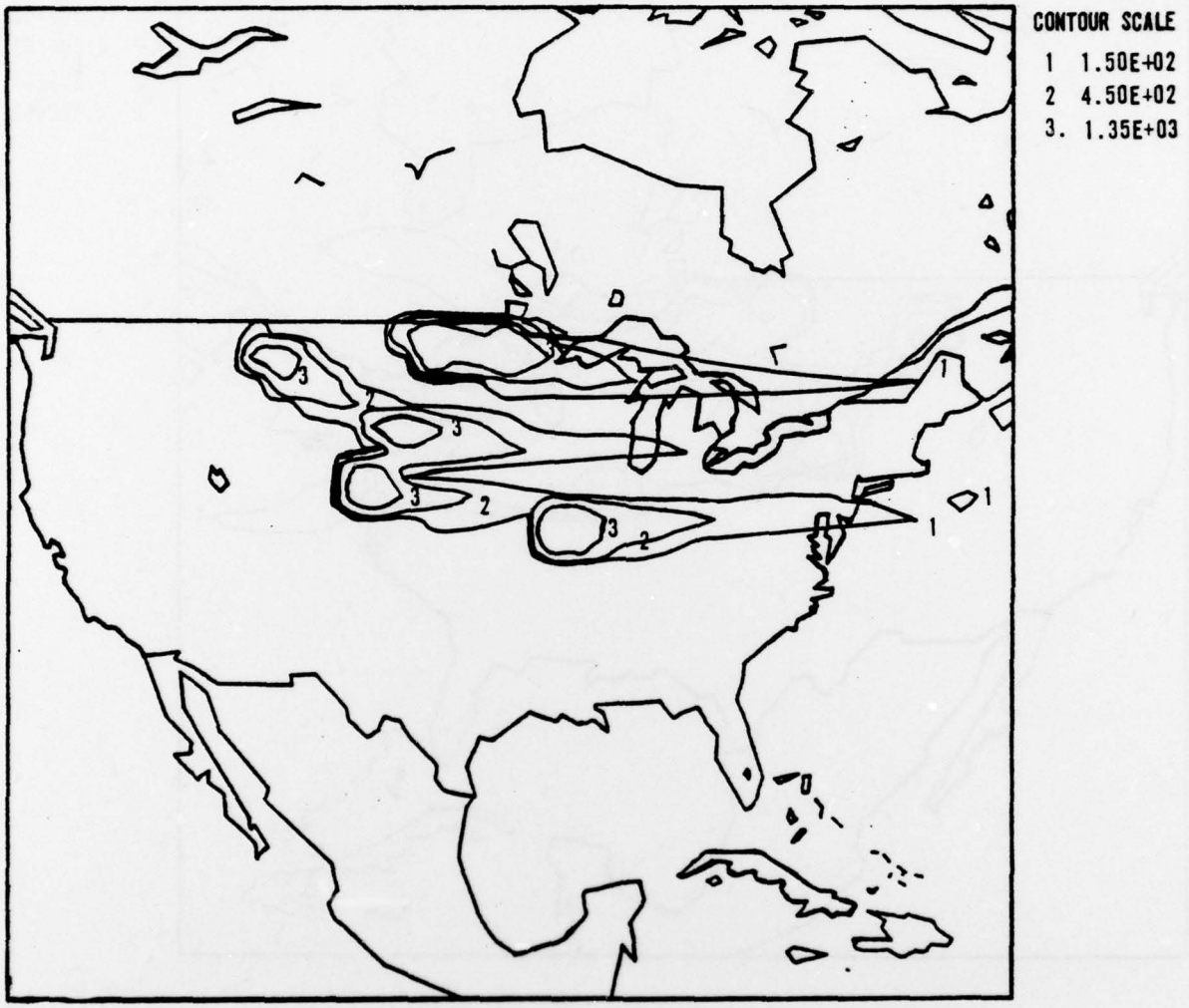

Figure 17. MM Mean Wind Dose at T = 10^8

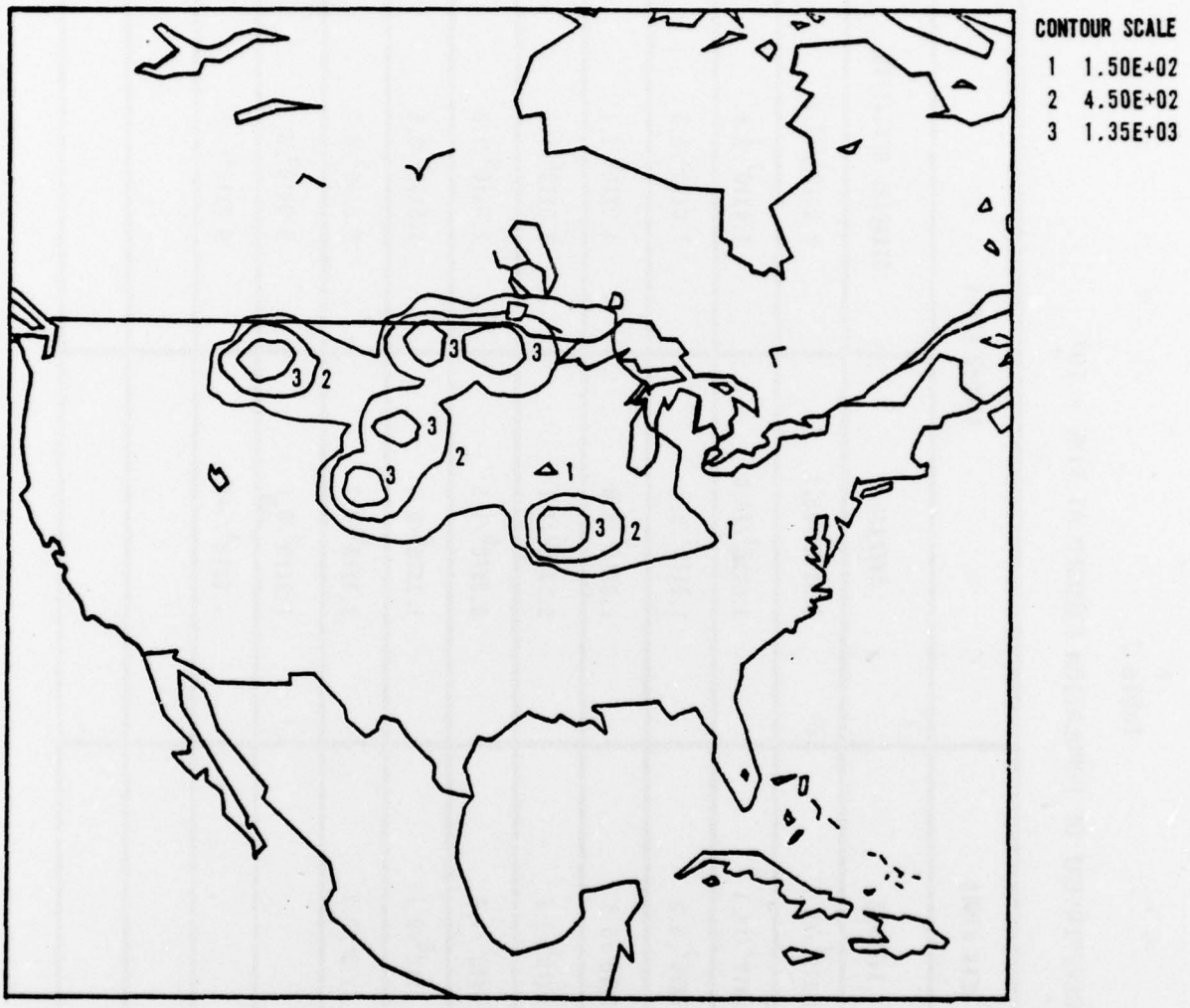

Figure 18. MM Mean Over Winds Dose at $T = 10^8$

Table 2

NUMBER/PERCENT OF POPULATION EXPOSED AT TIME = 10^8

MINIMUM DOSE (R)	MEAN WINDS	RANDOM WINDS	
	AVERAGE	AVERAGE	STANDARD DEVIATION
100	$9.5X10^7/46.7$	$7.3X10^7/35.7$	$2.6X10^7/12.8$
170	$3.9X10^7/19.1$	$3.0X10^7/14.8$	$1.4X10^7/6.8$
280	$1.7X10^7/8.5$	$1.7X10^7/8.6$	$7.8X10^6/3.8$
460	$1.2X10^7/5.8$	$1.0X10^7/5.0$	$4.9X10^6/2.4$
770	$5.5X10^6/2.7$	$5.5X10^6/2.7$	$2.6X10^6/1.3$
1300	$3.6X10^6/1.8$	$3.0X10^6/1.5$	$2.0X10^6/1.0$
2200	$1.5X10^6/0.7$	$1.3X10^6/0.6$	$9.5X10^5/0.5$
3600	$4.0X10^5/0.2$	$3.6X10^5/0.2$	$6.5X10^5/0.3$
6000		$1.3X10^5/0.1$	$5.0X10^5/0.2$
10000		$1.9X10^4/\sim 0$	$9.6X10^4/\sim 0$
130000			
1000000			

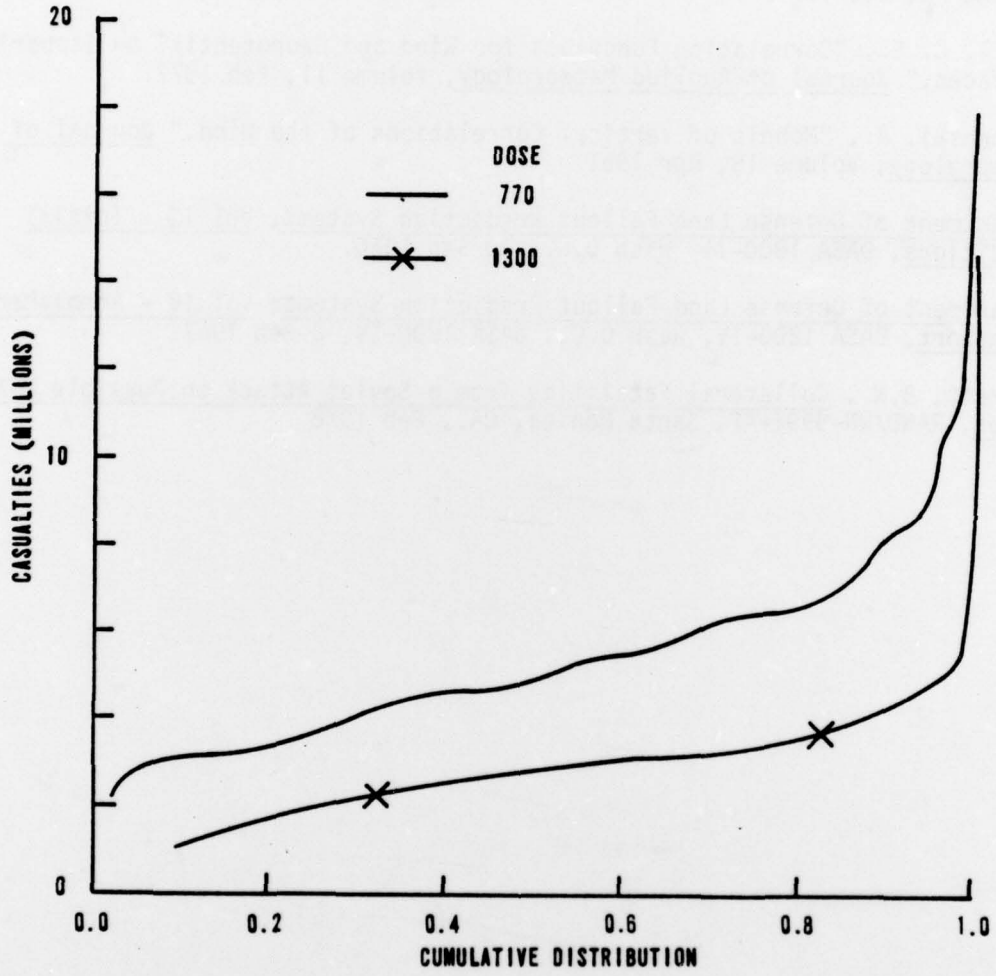

Figure 19. MM Cumulative Casualty Distribution

REFERENCES

1. Buell, C. E., "Two-Point Wind Correlations on an Isobaric Surface in a Nonhomogeneous Non-Isotropic Atmosphere," Journal of Applied Meteorology, Volume 10, Dec 1971.

2. Buell, C. E., "Correlation Functions for Wind and Geopotential on Isobaric Surfaces," Journal of Applied Meteorology, Volume II, Feb 1972.

3. Kochanski, A., "Models of Vertical Correlations of the Wind," Journal of Meteorology, Volume 18, Apr 1961.

4. Department of Defense Land Fallout Prediction Systems, Vol II - Initial Conditions, DASA 1800-II, Wash D.C., 30 Sep 1966.

5. Department of Defense Land Fallout Prediction Systems, Vol IV - Atmospheric Transport, DASA 1800-IV, Wash D.C., DASA 1800-IV, 2 Feb 1967.

6. Bennett, B.W., Collateral Fatalities from a Soviet Attack on Possible M-X Bases, RAND/WN-9991-AF, Santa Monica, CA., Feb 1978